

Article

Optimal Design of an Artificial Intelligence Controller for Solar-Battery Integrated UPQC in Three Phase Distribution Networks

Koganti Srilakshmi ¹, Canavoy Narahari Sujatha ², Praveen Kumar Balachandran ³, Lucian Mihet-Popa ^{4,*}
and Naluguru Udaya Kumar ⁵

- ¹ Department of EEE, Sreenidhi Institute of Science and Technology, Hyderabad 501301, India
² Department of ECE, Sreenidhi Institute of Science and Technology, Hyderabad 501301, India
³ Department of EEE, Vardhaman College of Engineering, Hyderabad 501218, India
⁴ Faculty of Information Technology, Engineering and Economics, Oestfold University College, 1757 Halden, Norway
⁵ Department of ECE, Marri Laxman Reddy Institute of Technology and Management, Domara Pocham Pally 500043, India
* Correspondence: lucian.mihet@hiof.no

Abstract: In order to minimize losses in the distribution network, integrating non-conventional energy sources such as wind, tidal, solar, and so on, into the grid has been proposed in many papers as a viable solution. Using electronic power equipment to control nonlinear loads impacts the quality of power. The unified power quality conditioner (UPQC) is a FACTS device with back-to-back converters that are coupled together with a DC-link capacitor. Conventional training algorithms used by ANNs, such as the Back Propagation and Levenberg–Marquardt algorithms, can become trapped in local optima, which motivates the use of ANNs trained by evolutionary algorithms. This work presents a hybrid controller, based on the soccer league algorithm, and trained by an artificial neural network controller (S-ANNC), for use in the shunt active power filter. This work also presents a fuzzy logic controller for use in the series active power filter of the UPQC that is associated with the solar photovoltaic system and battery storage system. The synchronization of phases is created using a self-tuning filter (STF), in association with the unit vector generation method (UVGM), for the superior performance of UPQC during unbalanced/distorted supply voltage conditions; therefore, the necessity of the phase-locked-loop, low-pass filters, and high-pass filters are totally eliminated. The STF is used for separating harmonic and fundamental components, in addition to generating the synchronization phases of series and shunt filters. The prime objective of the suggested S-ANNC is to minimize mean square error in order to achieve a fast action that will retain the DC-link voltage's constant value during load/irradiation variations, suppress current harmonics and power-factor enhancement, mitigate sagging/swelling/disturbances in the supply voltage, and provide appropriate compensation for unbalanced supply voltages. The performance analysis of S-ANNC, using five test cases for several combinations of loads/supply voltages, demonstrates the supremacy of the suggested S-ANNC. Comparative analysis was carried out using the GA, PSO, and GWO training methods, in addition to other methods that exist in the literature. The S-ANNC showed an extra-ordinary performance in terms of diminishing total harmonic distortion (THD); thus PF was improved and voltage distortions were reduced.

Keywords: fuzzy-logic controller; self-tuning filter; unified power quality conditioner; solar PV generation; battery system



Citation: Srilakshmi, K.; Sujatha, C.N.; Balachandran, P.K.; Mihet-Popa, L.; Kumar, N.U. Optimal Design of an Artificial Intelligence Controller for Solar-Battery Integrated UPQC in Three Phase Distribution Networks. *Sustainability* **2022**, *14*, 13992. <https://doi.org/10.3390/su142113992>

Academic Editors: Surender Reddy Salkuti and Brian Azzopardi

Received: 3 October 2022

Accepted: 23 October 2022

Published: 27 October 2022

Publisher's Note: MDPI stays neutral with regard to jurisdictional claims in published maps and institutional affiliations.



Copyright: © 2022 by the authors. Licensee MDPI, Basel, Switzerland. This article is an open access article distributed under the terms and conditions of the Creative Commons Attribution (CC BY) license (<https://creativecommons.org/licenses/by/4.0/>).

1. Introduction

Currently, distribution networks are prone to PQ issues such as interruptions, disturbances, flickering, sagging/swelling, harmonics, PF, and so on. This is due to a combination

of inconsistent behaviors involving wind, the tides, the sun, and so on, as well as large nonlinear and unbalanced loads being used with electronic power equipment; however, increased usage of large nonlinear industrial loads leads to a decline in PF, and therefore, maintaining PQ has become the primary challenge for engineers who work in the power industry. Various configurations of single and three phase SUAPFs, using various control techniques, were suggested for three and four wire distribution systems, for balanced and unbalanced supply voltages, in order to attend to PQ issues. In addition, the most recent developments and applications of SUAPFs were also discussed [1]. The novel controller, based on SRFT, was designed for the 3 ϕ -4 wire UPQC in order to effectively address the PQ issues for both the unbalanced and distorted loads of the distribution system [2].

A hybrid controller with a combination of FLC and PIC properties was developed for SUAPFs with the aim of reducing THD so that it aligned with the standard. To show the superiority of the proposed controller, case study analysis was conducted for balanced and unbalanced loads [3]. Moreover, a STF-based solar battery, which was connected to the SUAPF, was developed in order to efficiently regulate the reactive power and minimize the current harmonics. Additionally, the larger Kalman-type filter was used as a reference for the current assessment [4]. Furthermore, the improved performance of artificial intelligence-based controllers such as FLC, ANNC, and so on, for use with SUAPFs, were able to address PQ problems effectively, even when dynamic load changes occurred [5–7].

A solar integrated UPQC was developed, and its performance was tested on different load variations, using maximum power tracking, with the aim of diminishing THD and boosting the overall performance of UPQC [8]. Moreover, the SRFT-based PIC was designed for the fuel cell that supported the SUAPF, with the goal of effectively suppressing the current harmonics and regulating voltage across the DC-link [9]. A new controller, inspired by metaheuristic PSO and GWO-based algorithms, was suggested for the optimal tuning of the SUAPF, with the aim of managing the reactive power and minimizing the THD efficiently [10]; however, to regulate the voltage, and to control the reactive power at the grid, a feed forward training-based ANNC was implemented on a wind/solar associated UPQC [11].

A soccer league algorithm, based on the optimal tuning of a PI controller for a UPQC, was proposed to effectively address the PQ issues affecting the voltage and current [12]. Moreover, a multilevel UPQC, which was associated with the PV/wind and fuel cell, was proposed with the aim of efficiently eliminating voltage distortions and current harmonics [13]. The neuro-fuzzy-based hybrid controller was recommended for the UPQC in order to suppress the current harmonics and DC-link balancing in the distribution network for different loading conditions [14]. The soccer league algorithm's optimization-based load flow, which is suitable for both the transmission and distribution system, was formulated with the intention of minimizing the sum of the square of the active and reactive power mismatches for all of the buses [15].

The STF-based SUAPF was designed to eliminate the requirement of LPF and PLL and to reduce THD; moreover, to prove its viability, an investigation was conducted to find out whether its practical performance could match its theoretical performance [16]. The UPQC with a FL controller was suggested for non-linear R–L loads in order to suppress current harmonics, thereby reducing waveform imperfections. In addition, in order to gauge its superiority, analysis was undertaken on STF-based SUAPFs both with and without a UPQC [17]. A Fourier transform was recommended for solar, wind, fuel-cell, and battery-connected UPQCs, with the aim of eliminating voltage distortions in the supply voltage and reducing imperfections in the load current [18].

An adaptive, full order-based technique was suggested for the UPQC so that it could rapidly respond with a high accuracy for all dynamic load changes and grid conditions when faults were identified. Additionally, a BBO metaheuristic algorithm was used for optimally tuning the K_p/K_i of the PIC, with the goal of stabilizing the DC-link voltage oscillations [19].

The UPQC was employed to eliminate the voltage imbalances and to reduce imperfections in current harmonics, in addition to improving how the network was utilized, by using an adaptive, neuro-fuzzy hybrid controller [20]. A controller that used a hybrid of improved-bat and moth-flame algorithms was developed to deal with PQ issues, with the aim of reducing the power mismatch errors by appropriately tuning the K_p and K_i parameters [21].

The FL controller was suggested for the series active power filter, for the grid connected to the distribution network, in order to attend to PQ problems such as voltage imperfections and current harmonics, and to maintain the DC-link capacitor voltage [22].

The predator-prey-based firefly optimization technique was suggested for calculating the optimal K_p and K_i values of the PIC for the shunt active power filters, with the objective of minimizing THD and improving PF [23]; however, conventional training algorithms, such as the back propagation (BP) and Levenberg-Marquardt (LM) algorithms, delivered solutions based on local optima. Hence, the neural network was trained by the lightning search algorithm (LSA), which was proposed with the aim of solving real time problems [24]. The optimal tuning of PIC, based on the ant colony algorithm, was designed for the shunt active power filter, with the aim of minimizing THD under different loading conditions [25]. A hybrid fuzzy back control scheme was proposed for the five-level UPQC, with the intention to minimize the THD and improve the PF [26]. Ant-lion optimization-based training of feed forward ANNs was proposed to prevent solutions based on the local optima [27]. In addition, training ANNs via back propagation (BP) has certain drawbacks in that it provides local, rather than global, minima. Grey wolf-based training of feed forward neural networks was proposed to solve real time problems [28]. Moreover, an atom search optimization (ASO)-based UPQC was designed to solve PQ problems; this was achieved by integrating large renewable energy sources. In addition, a fractional order proportional integral derivative (FOPID) was introduced with ASO for solar-, wind-, and battery-integrated UPQCs, in order to effectively mitigate PQ issues [29].

The main contributions of this paper are as follows. The S-ANNC was proposed for use with the SUAPF, and the FLC was proposed for use with the SEAPF of the UPQC that was associated with the SPV system and BS system. These proposals were based on the idea that the current THD would be minimized, thereby enhancing the PF, maintaining stable DC-link voltage during load/solar irradiation variations, and enabling compensation to occur during sagging/swelling and disturbances as the minimization of the MSE would be considered an objective function. In addition, the STF-UVGM generated SYP for both SEAPF and SUAPF instead of PLL; however, STF also eliminates the necessity of LPFs and HPFs when the FC and HC of the current are separated. The performance analysis of the proposed S-ANNC, which would be used with the FLC-based controller so that the UPQC could be used with SPV and BS (U-SPBS) systems, was carried out for five different test cases. A comparative study was also conducted to exhibit the supremacy of the S-ANNC over the GA, PSO, and GWO trained methods, and other methods that exist in the literature.

The remainder of the paper is organized as follows. Section 2 details the construction of the proposed U-SPBS; Section 3 details the proposed S-ANNC; Section 4 presents the results and discussion; and Section 5 concludes the paper.

2. Construction of a UPQC with SPV and BS Systems (U-SPBS)

The configuration of the proposed U-SPBS is shown in Figure 1. The SPV and BS are integrated with the UPQC through a DC-link via a BC and BBC. The UPQC is composed of an arrangement of both series and shunt converters. The role of the SEAPF is to mitigate voltage related distortions such as sagging/swelling/disturbances and unbalanced supply voltage. Moreover, the isolation between the series converter and the power line is produced by injecting it into the transformers. In addition, it injects suitable V_{se} into the grid. Similarly, the main objective of the SUAPF is to suppress the harmonics in the current waveform by injecting a suitable i_{sh} and fast response in order to maintain the constant DC-link voltage

across the capacitor. The 3 ϕ balanced/unbalanced R–L loads and the induction furnace load were considered in this work.

The SPV and BS act as exterior supports for the DC-link of the UPQC, through a BC and BBC, in order to maintain stable voltage across the DC-link capacitor during load variations and to minimize converter ratings, as shown in Figure 2. The SPV and BS ratings considered in this work are listed in Table 1. The power distribution of U-SPBS at the DC-link is given in Equation (1).

$$P_{PV} + P_{BS} - P_{DC-Link} = 0 \tag{1}$$

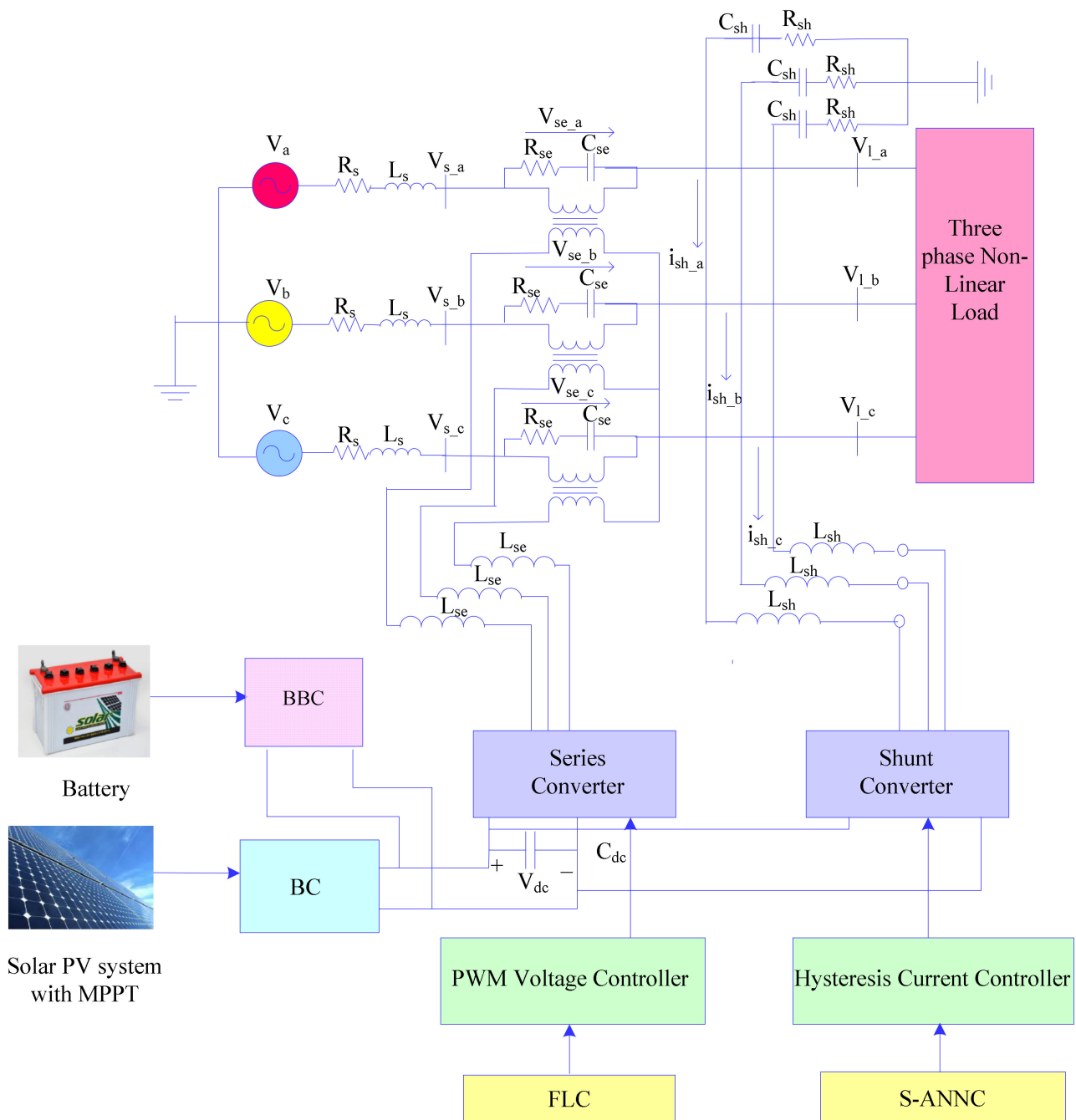


Figure 1. Components of a UPQC with SPV and BS systems (U-SPBS).

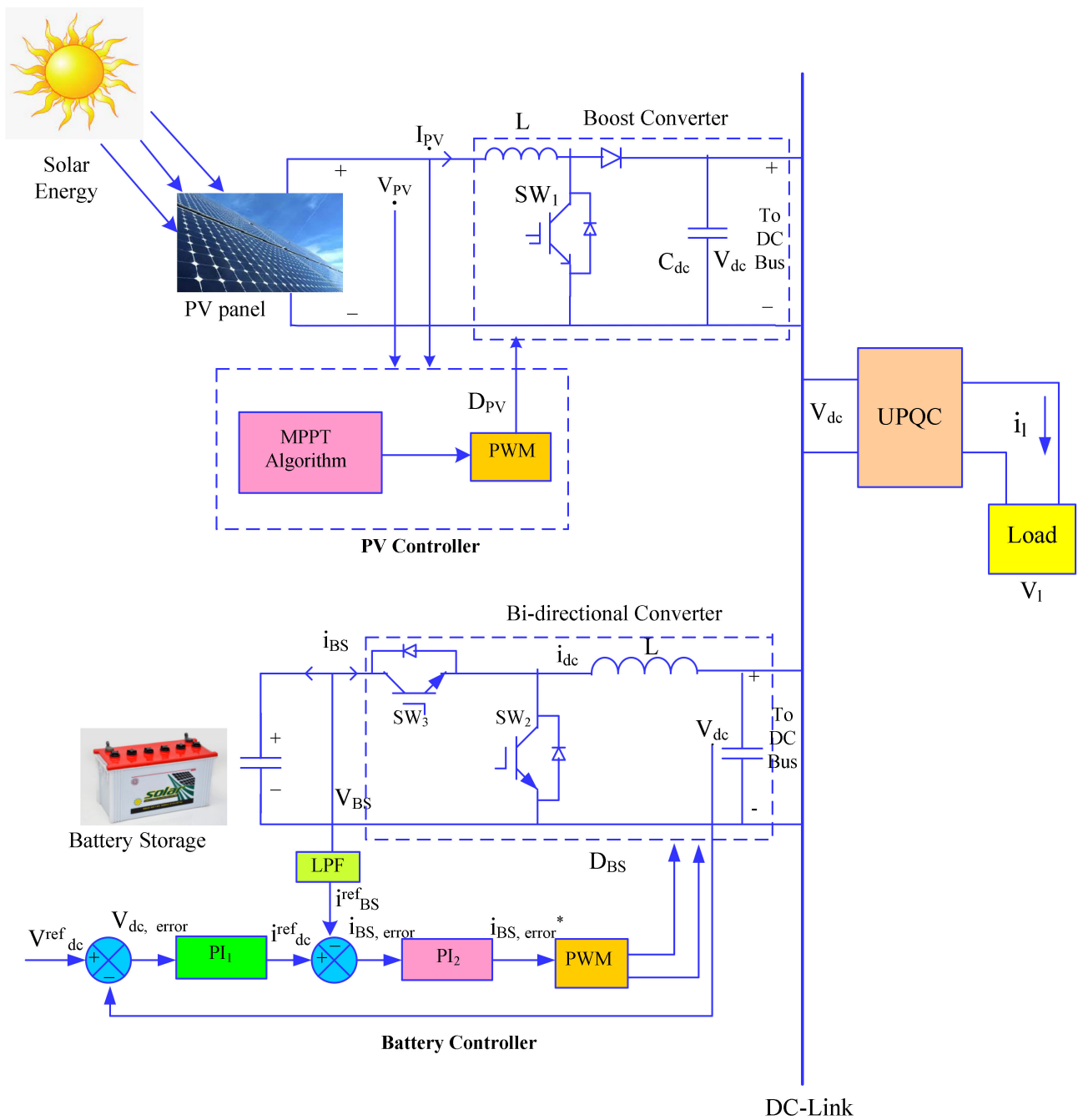


Figure 2. Proposed UPQC with PV and battery controllers.

Table 1. Solar-PV Panel and Battery Ratings.

Device	Parameters	Values
Solar-PV panel (SPR-215-WHT-U)	Output power	214.92 W
	Open circuit voltage	48.3 V
	Short circuit current	5.8 A
	Voltage/current at maximum power	39.80 V/5.40 A
	No. of PV cells connected in parallel	11
Li-ion battery	Rated Capacity	350 Ah
	Maximum capacity	450 Ah
	Nominal Voltage	650 V
	Fully charged voltage	755 V

2.1. SPV System

The SPV system converts solar irradiation into electrical energy. It consists of three PV panels connected in a series/parallel with the MPPT, and the BC is shown in Figure 2. The amount of solar power generation (SPG) depends on the amount of irradiation on the PV panels. Integrating the SPV system with the DC-link reduces voltage ratings, the stress on converters, and the demand on utility. The MPPT controller (perturb and observe) was implemented to extort highest level of productivity from the solar system. The output power P_{PV} is evaluated using Equation (2).

$$P_{PV} = V_{PV} \times I_{PV} \quad (2)$$

2.2. BS System

The BS controller contains a lead–acid type of battery that is connected to the BBC. It provides stable voltage across the DC-link, as shown in Figure 2. The $SOCB$ is calculated using Equation (3).

$$SOCB = 100(1 + \int i_{BS} dtQ) \quad (3)$$

The amount of power generated by the SPV decides the state of operation of a battery. It is either charged or discharged depending on whether it satisfies the upper or lower constraints, as shown in Equation (4).

$$SOCB_{\min} \leq SOCB \leq SOCB_{\max} \quad (4)$$

$K_{p1} = 0.7$, $K_{i1} = 10.1$, $K_{p2} = 2.77$, and $K_{i2} = 11.17$ gains are chosen arbitrarily. Table 2 shows the power distributions across the DC-link under various levels of SPG.

Table 2. Power sharing at the DC-link.

Intensity of SPG	Action
$SPG > P_{DC}$	Excess SPG is used to charge the battery until it reaches $SOCB_{\max}$
$SPG = P_{DC}$	The SPG alone will supply P_{DC}
$SPG < P_{DC}$	The difference in power is mediated by the battery until it reaches $SOCB_{\min}$
No SPG	BS alone supplies P_{DC}

3. Control Strategy of U-SPBS Using STF

When a fault or change in load occurs, the voltage across the capacitor of the DC-link varies; therefore, it is very important to ensure that the DC-link voltage is stable for a short period of time. In D-Q theory, currents and voltages are first transformed into a Clarke's reference. In general, a conventional UPQC mechanism consists of a SUAPF, SEAPF, and PLL. Moreover, the purpose of a PLL is to separate the positively sequenced components from the supply voltage; however, in this proposed system, the STF-UVGM would be used to generate SYP, using the distorted supply voltages, so that it could perform the same role as HPFs and LPFs in terms of separating the FC and HC of currents. Ergo, the suggested system consists of a STF, SUAPF, and a SEAPF. The switching of the series and shunt VSCs occurs when the PWM voltage and PWM hysteresis current controllers are being used with the S-ANNC. The major parts of the proposed control structure are detailed below:

3.1. Design Procedure of the STF

The integral parts of the SRFT were designed by Hong-Sock, as shown in Equation (5).

$$V_{xy}(t) = e^{j\omega t} \int e^{-j\omega t} U_{xy}(t) dt \quad (5)$$

where, U_{xy} and V_{xy} are the former and latter integral signals of the SRF. The transfer function $H(s)$ is shown in Equation (6), and it is found by implementing the Laplace transformation to Equation (6).

$$H(s) = \frac{V_{xy}(s)}{U_{xy}(s)} = \frac{s + j\omega}{s^2 + \omega^2} \quad (6)$$

Ensuring that STF obtains a constant k value has already been established; thus, $H(s)$ is shown in Equation (7).

$$H(s) = \frac{V_{xy}(s)}{U_{xy}(s)} = \frac{k(s + k) + j\omega_n}{(s + k)^2 + \omega_n^2} \quad (7)$$

By exchanging U_{xy} with $x_{\alpha\beta}(s)$, and $V_{xy}(s)$ with $x'_{\alpha\beta}(s)$, Equations (8) and (9) are obtained, as follows:

$$x'_\alpha = \left(\frac{k}{s}[x_\alpha(s) - x'_\alpha(s)] - \frac{\omega_n}{s} \cdot x'_\beta(s)\right) \quad (8)$$

$$x'_\beta = \left(\frac{k}{s}[x_\beta(s) - x'_\beta(s)] - \frac{\omega_n}{s} \cdot x'_\alpha(s)\right) \quad (9)$$

where, ω_n is the required frequency, and k is the gain. If k decreases, the accuracy when obtaining the output decreases and vice-versa; therefore, by using a STF control, as shown in Figure 3, distorted voltage/current signals can be obtained without any alteration to the magnitude or phase angle.

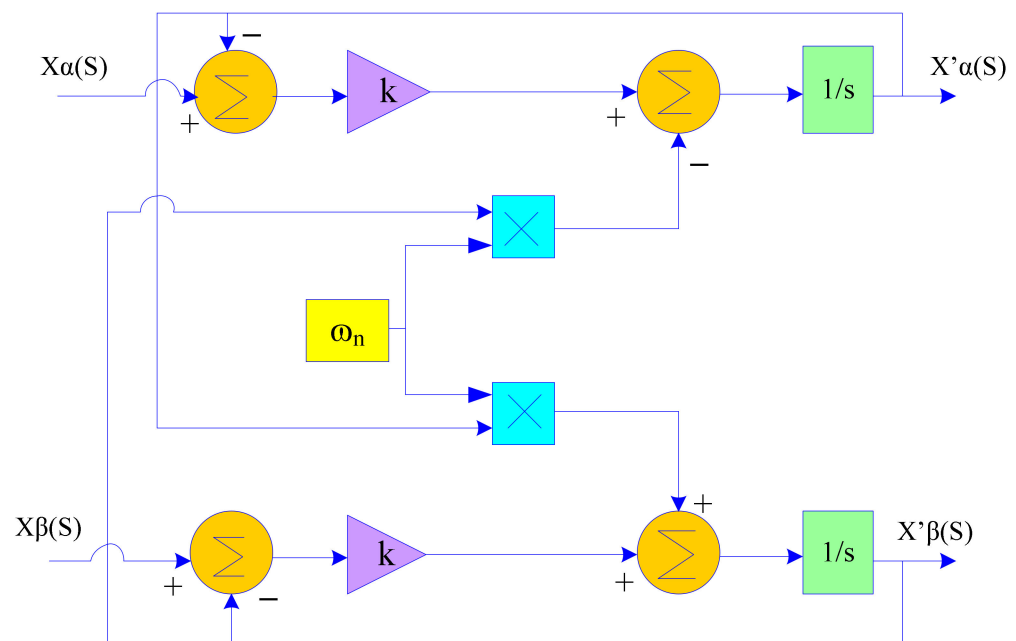


Figure 3. Controller of the STF.

This section may be divided into subcategories. They should provide a concise and precise description of the experimental results, their interpretation, as well as any experimental conclusions that can be drawn.

3.2. STF-UVGM for the Proposed U-SPBS

The suggested STF-UVGM is a non-iterative method which can provide SYP from the supply voltage, as shown in Figures 4 and 5. In Equation (10), the Clarke’s domain is used to transform the supply voltage from the *abc* to the $\alpha\beta 0$ domain.

$$\begin{bmatrix} V_{S_\alpha} \\ V_{S_\beta} \\ V_{S_0} \end{bmatrix} = \sqrt{\frac{2}{3}} \begin{bmatrix} 1 & -\frac{1}{2} & -\frac{1}{2} \\ 0 & \frac{\sqrt{3}}{2} & -\frac{\sqrt{3}}{2} \\ \frac{1}{2} & \frac{1}{2} & \frac{1}{2} \end{bmatrix} \begin{bmatrix} V_{S_a} \\ V_{S_b} \\ V_{S_c} \end{bmatrix} \tag{10}$$

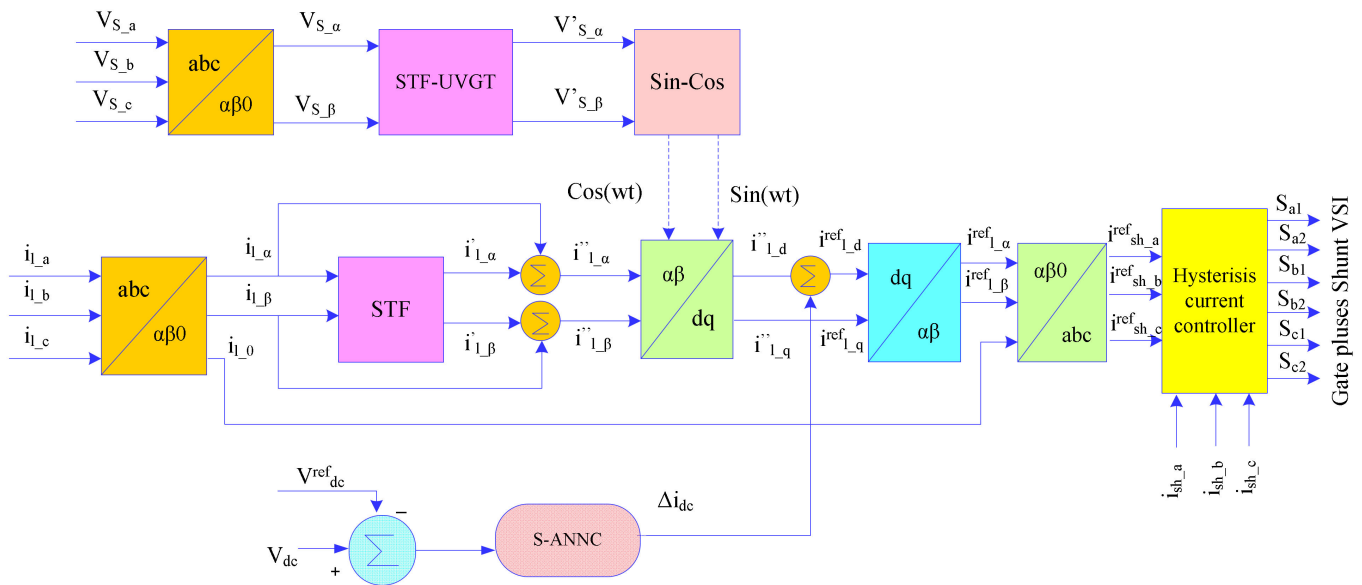


Figure 4. S-ANNC for the Shunt Converter.

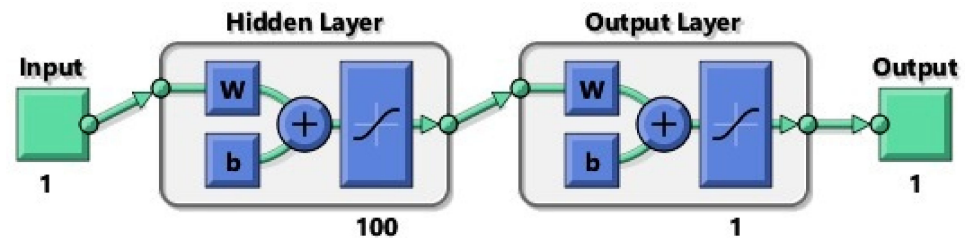


Figure 5. Structure of the ANNC for the DC-link.

The FC and HC are separated from the distorted grid voltages, as noted in Equation (11), by only considering the $\alpha\beta$ domain.

$$\begin{bmatrix} V_{S_\alpha} \\ V_{S_\beta} \end{bmatrix} = \begin{bmatrix} V'_{S_\alpha} + V''_{S_\alpha} \\ V'_{S_\beta} + V''_{S_\beta} \end{bmatrix} \tag{11}$$

Here, V'_{S_α} indicates the FC, and V''_{S_α} indicates the HC, in the $\alpha\beta$ domain. The STF suppresses the HC in the distorted grid voltages and extracts the FC to produce SYP with high quality. The Laplace transformation of STF is expressed in Equation (12).

$$\begin{bmatrix} V'_{S_\alpha}(s) \\ V'_{S_\beta}(s) \end{bmatrix} = \frac{k1}{s} \begin{bmatrix} V_{S_\alpha}(s) - V'_{S_\alpha}(s) \\ V_{S_\beta}(s) + V'_{S_\beta}(s) \end{bmatrix} + \frac{2\pi fc1}{s} \begin{bmatrix} V'_{S_\beta}(s) \\ -V'_{S_\alpha}(s) \end{bmatrix} \tag{12}$$

where, $k1$ is the chosen gain, with a value of 20, and $fc1$ is the cut-off frequency, with a value is equal to the system’s frequency, at 50 Hz. The SYP’s $\sin(\omega t)$ and $\cos(\omega t)$ are

generated from Equation (13) which omits PLL. STF-UVGM effectively generates SYP for distorted supply voltage of U-SPBS.

$$\begin{bmatrix} \sin(\omega t) \\ \cos(\omega t) \end{bmatrix} = \frac{1}{\sqrt{(V'_{S-\alpha})^2 + (V'_{S-\beta})^2}} \begin{bmatrix} V'_{S-\alpha} \\ -V'_{S-\beta} \end{bmatrix} \quad (13)$$

3.3. Shunt Controller

The main function of the SUAPF is to suppress the current harmonics by injecting the required amount of current and to regulate the DC capacitor in order to keep the voltage stable. The shunt controller adapts the (i) $abc-\alpha\beta 0$, $\alpha\beta 0-dq$, $dq-\alpha\beta 0$, and $\alpha\beta 0-abc$ transformations; and (ii) S-ANNC is implemented to minimize the THD and regulate the DC-link voltage so that it remains stable. The proposed S-ANNC compares the actual voltage of the DC-link with the reference voltage, and it transfers the error (current output) into the axis. The controller of the S-ANNC is shown in Figure 4. As the $abc-\alpha\beta 0$, $\alpha\beta 0-dq$, $dq-\alpha\beta 0$, and $\alpha\beta 0-abc$ transformations are already available in the literature, the design of the S-ANNC is shown in Figure 5.

Initially, in the SUAPF, the load currents are shifted to $\alpha - \beta - 0$ coordinates by using the Clarke transformation. By performing the Laplace conversion, the STF splits the HC from the FC. As a result of the HC obtained from the $\alpha - \beta - 0$ coordinates, and the SYP obtained from Equation (18), the HC in the d-frame is able to be obtained. The reference for the current generation and stable DC-link voltage plays a vital role in determining the performance of the SUAPF; however, if the load changes, the active power flow in the SUAPF may vary, which leads to voltage instability across the DC-link. To regulate the voltage across the DC-link, the active power in the SUAPF is made equal to the switching losses. The suggested S-ANNC injects an appropriate error current signal, Δi_{dc} , which is obtained from the difference between the actual and reference DC-link voltages. The mathematical expression for the calculation of the DC-link voltage is shown in Equation (14).

$$\Delta i_{dc} = e_1(t) = V^{ref}_{dc} - V_{dc}(t) \quad (14)$$

The reference load current in the d -axis can be calculated using Equation (15).

$$i^{ref}_{l,d} = i''_{l,d} - \Delta i_{dc} \quad (15)$$

The $d - q$ reference load currents are transformed into an $\alpha - \beta$ domain. Then, the reference shunt injected currents are transformed into an abc domain. The errors that the currents obtain from the comparison between the actual and reference signals are transferred to a hysteresis control in order to produce appropriate gating pulses.

3.3.1. Proposed S-ANNC

ANNs are featured among the more the famous artificial intelligence techniques. An ANN is a human-inspired mathematical model, and it is very adaptable in terms of its application to electronic power system controls. MLPs are familiar neural networks. The advantages of ANNs include its ability to self-learn, its fault tolerance, fast convergence, robustness, and so on. The architecture of an ANN consists of three layers, which are IL, HL, and OL. The most significant factor that affects the performance of an ANN is the learning algorithm that is selected for its training. Training is the process of searching for the best group of weights that links the neurons between the layers of the ANN to reduce error. Training methods for MLP networks mainly consist of two types: supervised and unsupervised. In general, these methods consist of two types, which are gradient search and meta-heuristic. BP is the most famous gradient-based conventional training method that is adopted for MLP networks. Even though the BP method is famous, it suffers from a few limitations: it provides a poor initial guess with regard to the weights, it has a slow convergence time, and its chances of getting trapped in local minima are high. Moreover,

meta-heuristic algorithm-based search methods depend on the random selection of initial guesses during their optimization process. The benefit of using these methods is that they find the best global optimal solution rather than the local optimal solution; however, they do need prior information concerning the chosen problem, and their main limitation is the computational time. These algorithms can be applied for the weight, parameter, and architecture optimization of an ANN. The aim of supervised learning is to diminish the error between the desired and output values.

In MLP networks, neurons between the layers are interrelated via numerical weights, and each neuron consists of summation and activation functions. The purpose of a summation function is to sum up the product of inputs and weights, as well as bias, as shown in Equation (16), where w_{pk} is the connection weight connecting I_p to neuron k , β_k is a bias term, and m is the total number of neuron inputs. Usually, a nonlinear activation function, such as a sigmoid function, is used; this is shown in Equation (17). Therefore, the output of neuron k can be described as per Equation (18).

$$S_k = \sum_{p=1}^m w_{pk} I_p + \beta_k \quad (16)$$

$$f(x) = \frac{1}{1 + e^{-x}} \quad (17)$$

$$O_k = f_k \left(\sum_{p=1}^m w_{pk} I_p + \beta_k \right) \quad (18)$$

In the proposed work, a single layer, feed-forward ANN is trained for DC-link balancing. V_{dc}^{ref} is compared with V_{dc} , and its error is taken as the input data, whereas the desired output, Δi_{dc} , is taken as the target data for the ANN. Figure 5 shows the ANN structure for the DC-link with 100 neurons in the HL. Figure 6 shows the architecture of the S-ANN controller for the DC-link. It was proven in [29] that a MLP network with a single hidden layer is adequate for the approximation of any function. The optimal selection of weights provides a much better performance than the selection of network architectures and activation functions. Overfitting is one major problem of neural networks, though it can be overcome by reducing the complexity of the network, ensuring that stopping early is used regularly, and so on. In this work, in order to reduce the complexity and number of parameters of the network, a single layer was used.

3.3.2. Soccer League Optimization (SLO)

SLO is a population-based sports algorithm that is derived from the competitive behavior within a team of players, and between other teams in the league. The performance of each player can be improved by competing with another player, thus improving the strength of the team. This paper provides an overview of a soccer league optimization-trained ANN.

The selection of weights can be treated as an optimization problem. Given that the aim is to minimize the value of the common mean squared error (MSE), the optimum parameters, $w_{1,1} \dots w_{1,50}, \dots w_{1,100}, W_1, \dots W_{50}, \dots W_{100}, \beta_0, \dots \beta_{50}, \dots \beta_{100}$, are chosen, and the fitness function is formed. With this approach, each player (y) is treated as a selected design parameter (weights) that is represented in a vector form, as shown in Equation (19).

$$y = [w_{1,1} \dots w_{1,50}, \dots w_{1,100}, W_1, \dots W_{50}, \dots W_{100}, \beta_0, \dots \beta_{50}, \dots \beta_{100}] \quad (19)$$

The constraints are represented as

$$y^k(\min) \leq y^k \leq y^k(\max); k = 1, 2, \dots, nd \quad (20)$$

where, nd = number of design variables.

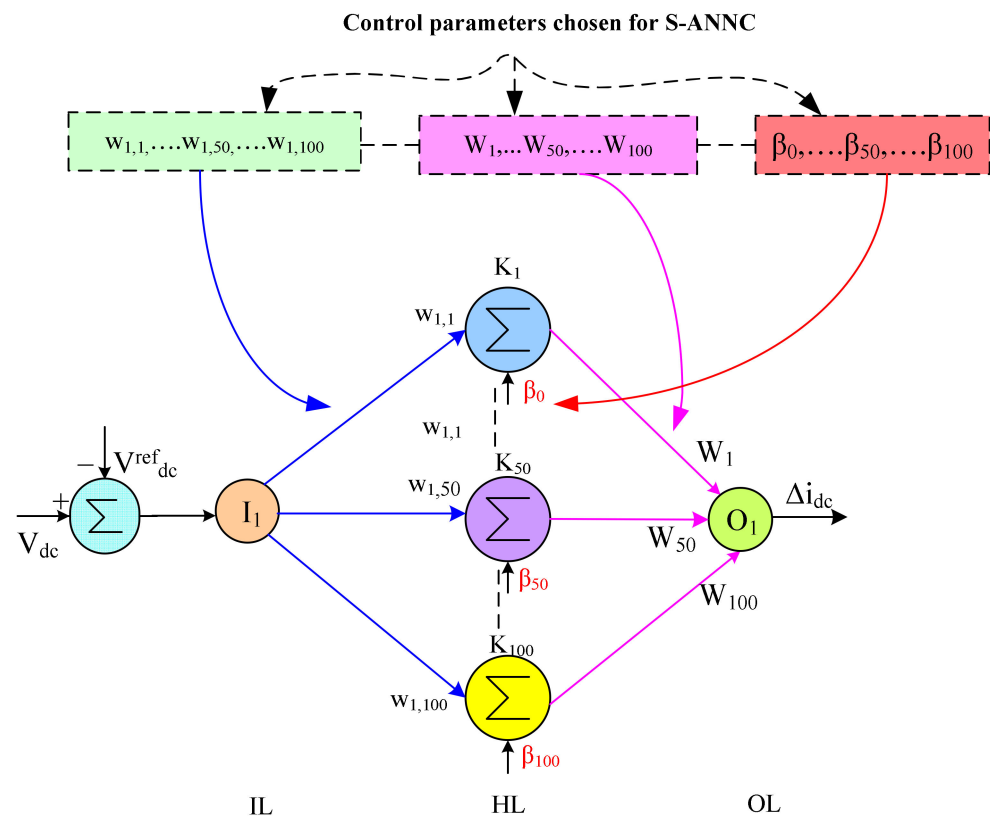


Figure 6. Architecture of the S-ANNC controller for the DC-link.

The total number of players is randomly produced and clustered into a certain number of teams. Each team consists of a set of active players (APLs), and substitute players (SPLs). In any team, each player has his/her own skills which are represented in Equation (21).

$$[y_{kj}^1, y_{kj}^2, \dots, y_{kj}^{nd}] = [w_{1,1} \dots w_{1,50}, \dots w_{1,100}, W_1, \dots W_{50}, \dots W_{100}, \beta_0, \dots \beta_{50}, \dots \beta_{100}] \quad (21)$$

The total number of players (population) and their teams (T) are denoted as,

$$Population = \left[\begin{array}{l} T_1 \rightarrow AT_1 = \left\{ \begin{array}{l} APL_{1,1} \\ APL_{1,2} \\ \vdots \\ APL_{1,nap} \end{array} \right\}; ST_1 = \left\{ \begin{array}{l} SPL_{1,1} \\ SPL_{1,2} \\ \vdots \\ SPL_{1,nspl} \end{array} \right\} \\ T_2 \rightarrow AT_2 = \left\{ \begin{array}{l} APL_{2,1} \\ APL_{2,2} \\ \vdots \\ APL_{2,nap} \end{array} \right\}; ST_2 = \left\{ \begin{array}{l} SPL_{2,1} \\ SPL_{2,2} \\ \vdots \\ SPL_{2,nspl} \end{array} \right\} \\ \vdots \\ T_m \rightarrow AT_m = \left\{ \begin{array}{l} APL_{m,1} \\ APL_{m,2} \\ \vdots \\ APL_{m,nap} \end{array} \right\}; ST_m = \left\{ \begin{array}{l} SPL_{m,1} \\ SPL_{m,2} \\ \vdots \\ SPL_{m,nspl} \end{array} \right\} \end{array} \right] \quad (22)$$

where,

$APL_{k,j}$ is the j th APL of k th team.

$SPL_{k,j}$ is the j th SPL of k th team.

nap and $nspl$ denote the number of APLs and SPLs, respectively.

AT_k is the k th active team with nap .

ST_k is the k th substitute team with nsp .

nd denotes the total number of control variables.

m denotes the number of teams.

In each team, the fitness of each player depends on his/her skills, which is calculated using a performance function (FF_{kj}) that is derived from the objective function (minimization of the MSE of the ANN), as shown below:

$$MaxFF_{kj} = \frac{1}{1 + MSE} \quad (23)$$

where the MSE is evaluated using Equation (24), O is the actual output, \bar{O} indicates the predicted output, and n is the total number of instances.

$$MSE = \frac{1}{n} \sum_{p=1}^m (O_p - \bar{O}_p)^2 \quad (24)$$

The likelihood of a team winning the league depends on the strength of the players. The strength of the k th team (ST_k) can be calculated using Equation (25).

$$ST_k = \sum_{j=1}^{nap+nsp} \frac{FF_{kj}}{nap+nsp} \quad (25)$$

The player that has the best fitness value in each (k th) team is considered to be the team leader (TL_k), and the best player among all team leaders, is called the super player (SuperPL) of the league. The probability of the k th team winning against the q th team is shown in Equation (26).

$$\left\{ \begin{array}{l} \text{if } rand() < \left(\frac{ST_k}{ST_k + ST_q} \right), \\ \text{k - th team is winner \& q - th team is loser} \\ \text{else} \\ \text{k - th team is loser \& q - th team is winner} \\ \text{end} \end{array} \right\} \quad (26)$$

Once the match is completed, the players of winning team and losing team implement certain actions to enhance their performance. The mathematical representation of these actions may be shown as a series of operators, as detailed below.

Imitation operator: the APLs of the winning team try to imitate the TL and SuperPL in order to enhance their own performance, as shown in Equations (27) and (28).

$$APL_{kj} = \mu_1 APL_{kj} + \tau_1 (SuperPL - APL_{kj}) + \tau_2 (TL_k - APL_{kj}) \quad (27)$$

$$APL_{kj} = \mu_2 APL_{kj} + \tau_1 (SuperPL - APL_{kj}) + \tau_2 (TL_k - APL_{kj}) \quad (28)$$

where, μ_2 , μ_1 , τ_1 , and τ_2 are random numbers.

If the performance of the APLs is improved, then the APL_{kj} can perform large movements, in accordance with Equation (27). Alternatively, the player shifts towards medium movements, in accordance with Equation (28). If there is no improvement after the above-mentioned actions have been taken, the player will remain in their previous position.

Provocation operator: The SPLs try to perform better than the APLs of the winning team. The SPLs move in accordance with the average direction of the APLs, using Equations (29) and (30).

$$SPL_{kj} = D(k) + \chi_1 (D(k) - SPL_{kj}) \quad (29)$$

$$SPL_{kj} = D(k) + \chi_2 (SPL_{kj} - D(k)) \quad (30)$$

where χ_1 , and χ_2 are random numbers.

$D(k)$ is the mean direction of the APLs in the winning team.

SP_{kj} is the j th substitute of k th team.

If the performance of the APLs is better than the old one, then the SPL_{kj} moves forward, in the average direction of APLs, using Equation (29). Alternatively, the player moves backwards, as per Equation (30). If there is no performance improvement after the abovementioned movements have been completed, he/she is replaced with a vector that has a random solution.

Mutation operator: The APLs of the losing team try to explore possible ways to enhance their performance. During this process, they randomly change their positions by adopting the mutation operator.

Substitution Operator: To escape from local traps, the losing team creates a fresh combination of substitutes (j and p) by integrating two of the existing members, as per Equations (31) and (32).

$$SPL_{kj} = \alpha SPL_{kj} + (1 - \alpha) SPL_{kp} \quad (31)$$

$$SPL_{kp} = \alpha SPL_{kp} + (1 - \alpha) SPL_{kj} \quad (32)$$

where, α is a random number. The chosen parameters of the soccer league algorithm are given in Table 3. The flowchart of the proposed design method is shown in Figure 7. An advantage of S-ANNC is its ability to quickly converge with fewer numbers of iterations that are used for both linear and nonlinear loads, and multi-objective problems.

Table 3. Chosen parameters.

Algorithm	Parameter	Chosen Value
SLO	Nap	6
	Nsp	4
	M	4

3.4. Series Controller

The main purpose of the SEAPF is to eliminate voltage-related PQ issues by injecting an appropriate voltage through the interfacing transformer. As the source and load voltages transform from abc to $\alpha - \beta - 0$, and then to $d - q$, and as two such voltage transformations are already noted in the literature, the design of the FLC as a reference for voltage generation is discussed in this paper. The reference series injected a voltage that was obtained from the difference between the actual reference source and the load voltage. The injected series voltage passes through the PWM voltage controller in order to generate the required pulses for the SEAPF, as shown in Figure 8.

FLC for Reference Voltage Generation

The FL is an intelligent controller which functions by using linguistic rules. The main components of an FL system are a fuzzifier, a rule base, knowledge base, an inference, and a defuzzifier. The fuzzifier converts numerical inputs into linguistic variables with the support of the MF. The knowledge base stores the updated information concerning all of the input–output relationships. Then, the inference determines the rule base and the MF of the fuzzifier. Lastly, the defuzzifier converts the fuzzy variables into a crisp output. The flow of the FL is illustrated in Figure 9. The Takagi–Sugeno method was considered for the proposed work, as it takes the E and CE as inputs for the system (where E is obtained from Equation (33)). The triangle MFs concerning the E, CE, and output are shown in Figures 10–12. The fuzzy variables are represented by a triangular MF, as shown in Figures 10–12. They include the HP, medium positive (MP), LP, Zero (ZO), HN, medium

negative (MN), and LN. The load voltage values are considered to be in the range of these linguistic terms, with 49 sets of MFs, as shown in Table 4.

$$E = V^{ref}_d - V^i_{l,d}; i = 1, 2, 3, 4, 5, 6 \tag{33}$$

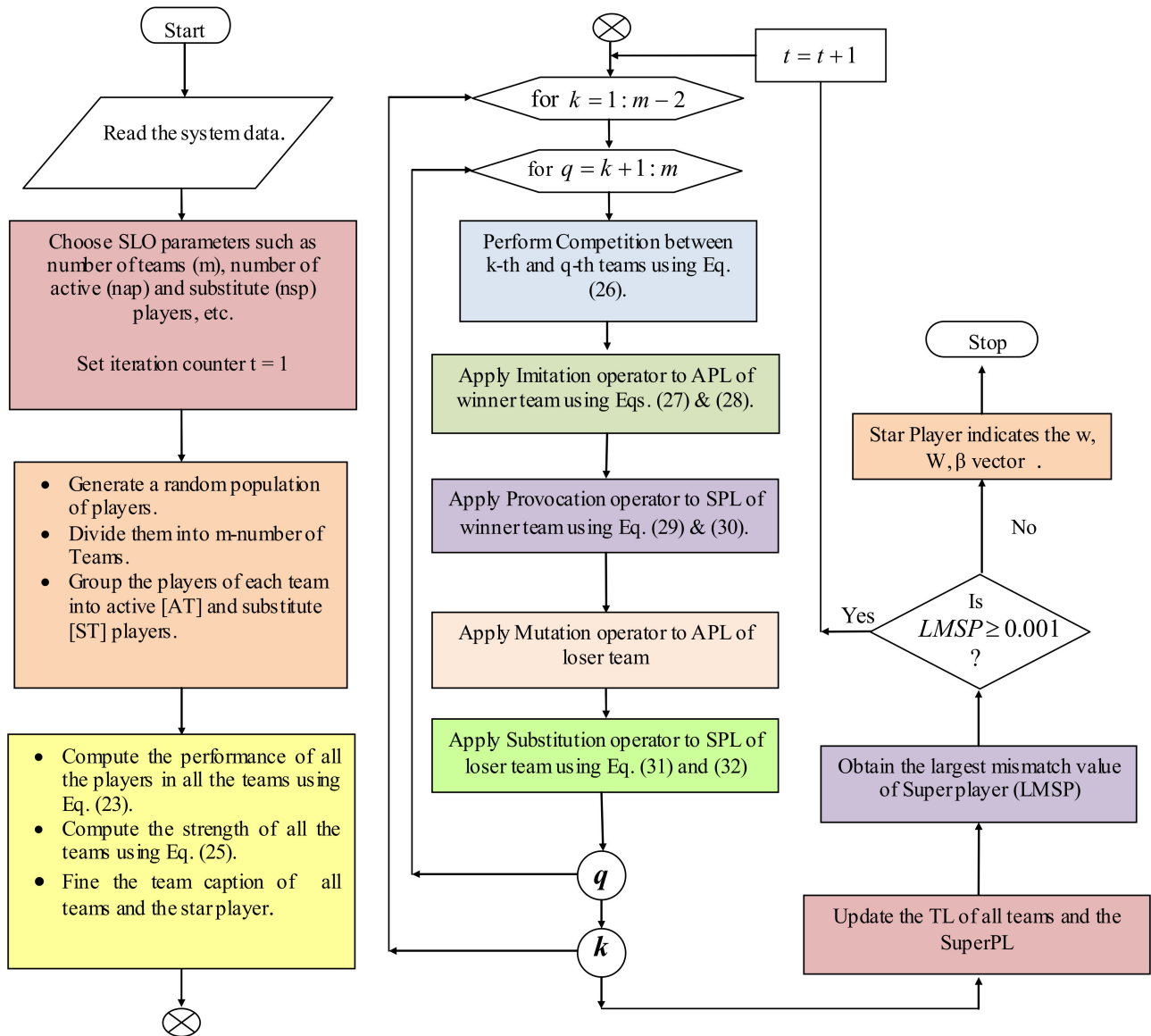


Figure 7. Flowchart of the soccer league algorithm-trained artificial neural network controller (S-ANNC).

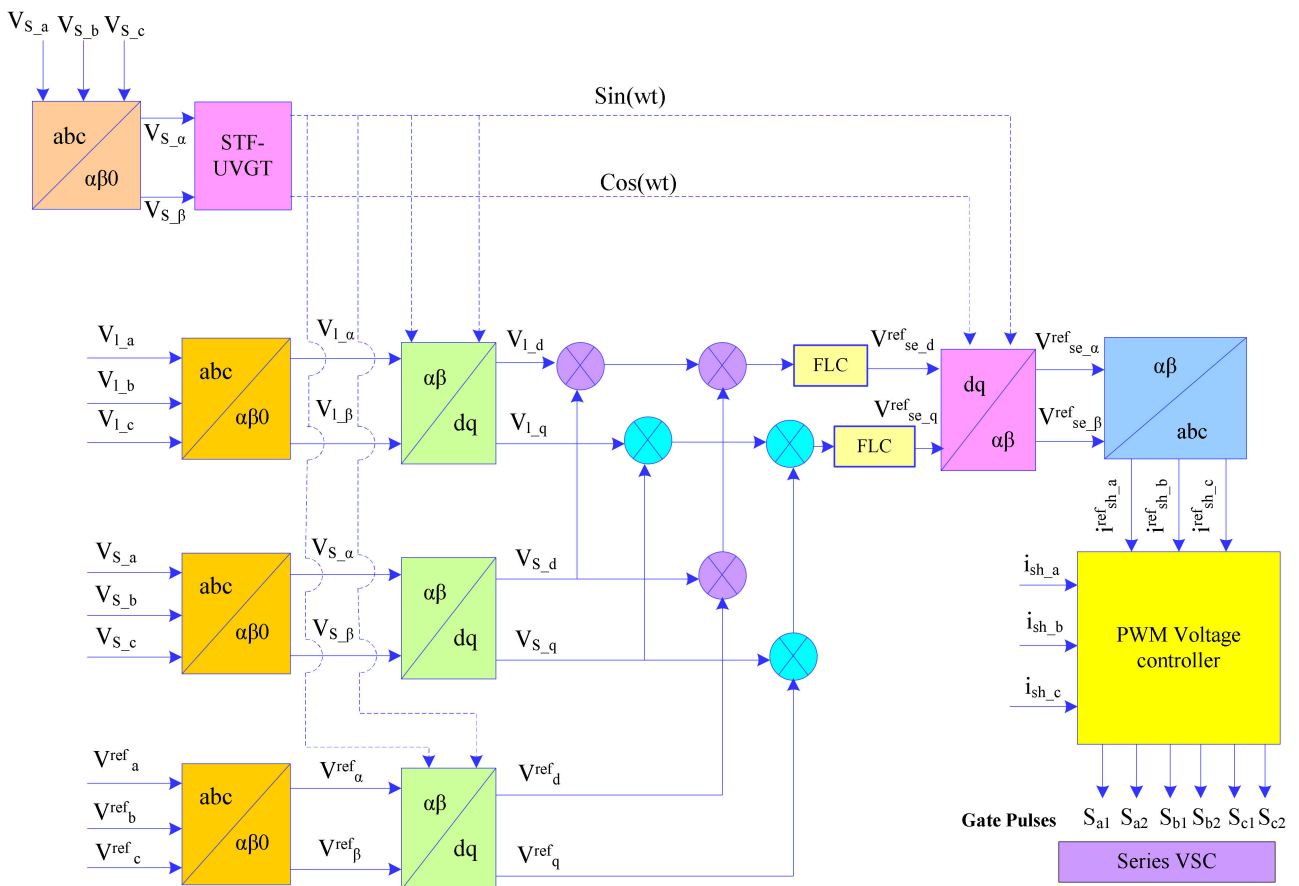


Figure 8. Series controller.

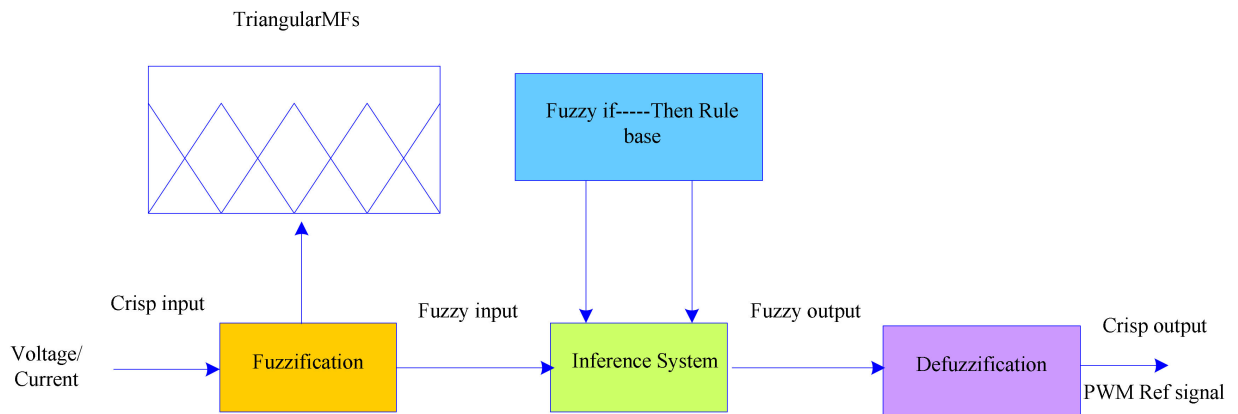


Figure 9. Process of the FLC.

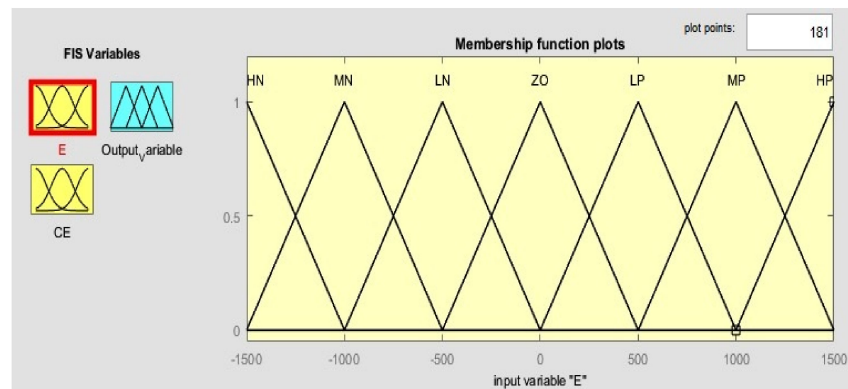


Figure 10. MF of “E”.

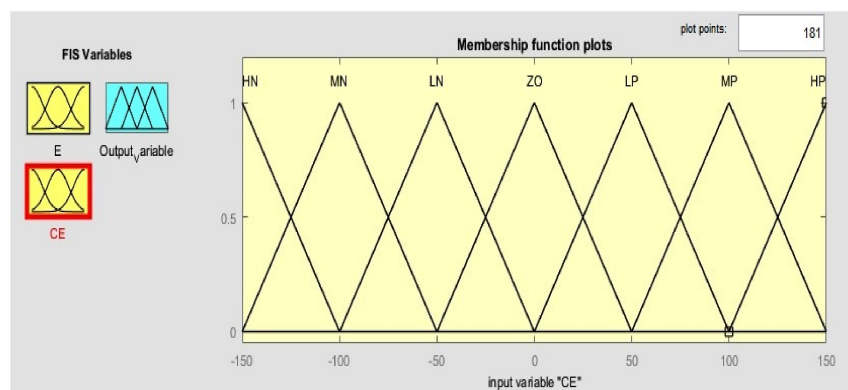


Figure 11. MF of “CE”.

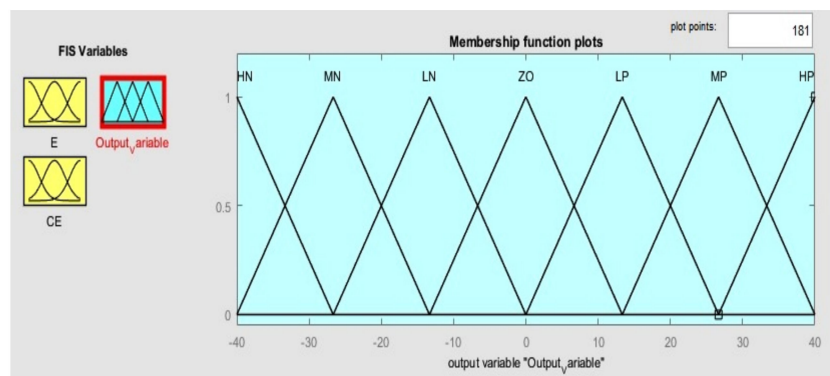


Figure 12. MF of the “Output duty cycle”.

Table 4. MF mapping for voltage errors.

Er	CE						
	HP	MP	LP	ZO	LN	MN	HN
HN	ZO	LN	MN	HN	HN	HN	HN
MN	LP	ZO	LN	MN	HN	HN	HN
LN	MP	LP	ZO	LN	MN	HN	HN
ZO	HP	MP	LP	ZO	LN	MN	HN
LP	HP	HP	MP	LP	ZO	LN	MN
MP	HP	HP	HP	MP	LP	ZO	LN
HP	HP	HP	HP	HP	MP	LP	ZO

4. Simulation and Results

To analyze the performance efficiency of the suggested controller of a U-SPBS, a 3 ϕ distribution system was selected. The U-SPBS and load specifications are shown in Table 5. The proposed system’s model was created in MATLAB/Simulink version 2016, using the SPS toolbox, as shown in Figure 13. The proposed algorithm was repeated 20 times, and the best output was represented as the optimal solution. Five test studies were considered in order to attest to the extraordinary performance of S-ANNC on the proposed U-SPBS, as shown in Table 6. These studies included multiple combinations of balanced/unbalanced/non-linear loads, supply voltages, variable irradiation, and conditions such as swelling/sagging/disturbances, under constant irradiation conditions of 1000 W/m² and a temperature of 25 °C.

Table 5. Ratings of U-SPBS.

Source	$V_s:: 50 \text{ Hz}; R_s: 0.1 \Omega; L_s: 0.151 \text{ mH}$
SEAPF	$R_{se}: 1 \Omega; L_{se}: 3.6 \text{ mH}; C_{se}: 60 \mu\text{F}$
SUAPF	$R_{sh}: 0.00101 \Omega; L_{sh}: 2.15 \text{ mH}; C_{sh}: 1.0 \mu\text{F}; \text{Hysteresis-band: } 0.01 \text{ A}$
DC-Link	$C_{dc}: 9400 \mu\text{F}; V_{dc}: 700 \text{ V}$

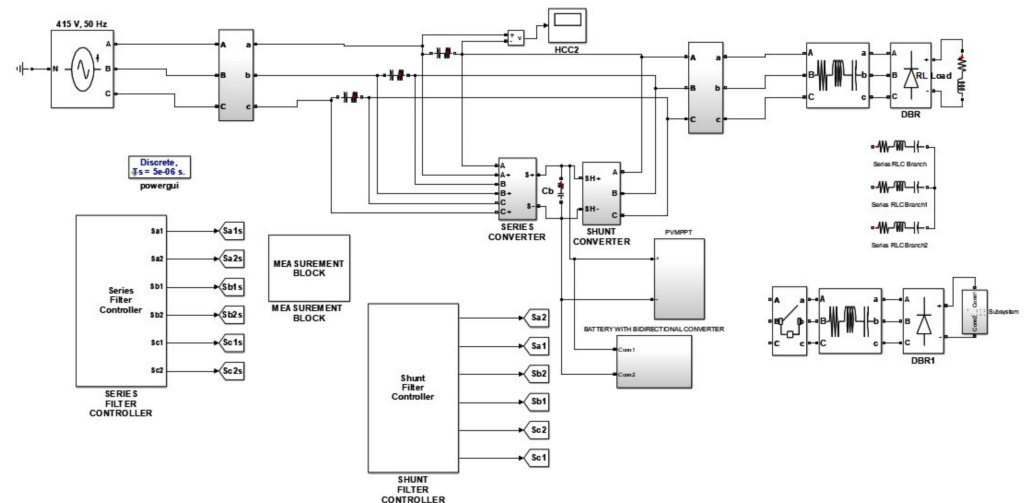


Figure 13. U-SPBS model with loads in the Simulink.

Table 6. Test cases considered under constant irradiation conditions of 1000 W/m² and temperature of 25 °C.

Condition/Load	Case1	Case2	Case3	Case4	Case-5
Balanced source voltage	✓	✓	✓		
Unbalanced source voltage				✓	✓
Voltage sagging, swelling, and disturbance	✓	✓	✓		
Steady state current	✓	✓	✓	✓	✓
Steady state voltage				✓	✓
Balanced Rectifier Load: 30 Ω and 20 mH	✓	✓	✓		✓
Unbalanced R–L Load: R: 10, 20, and 15 ohm; L: 9.50 mH, 10.50 Mh, and 18.50 mH		✓	✓	✓	
Induction Furnace load: LC = 400 mH, 50 μ F, RL = 10 ohm, 100 mH			✓		✓

Figure 14 shows the convergence characteristics of the S-ANNC with those of the GA, PSO, and GWO trained controllers.

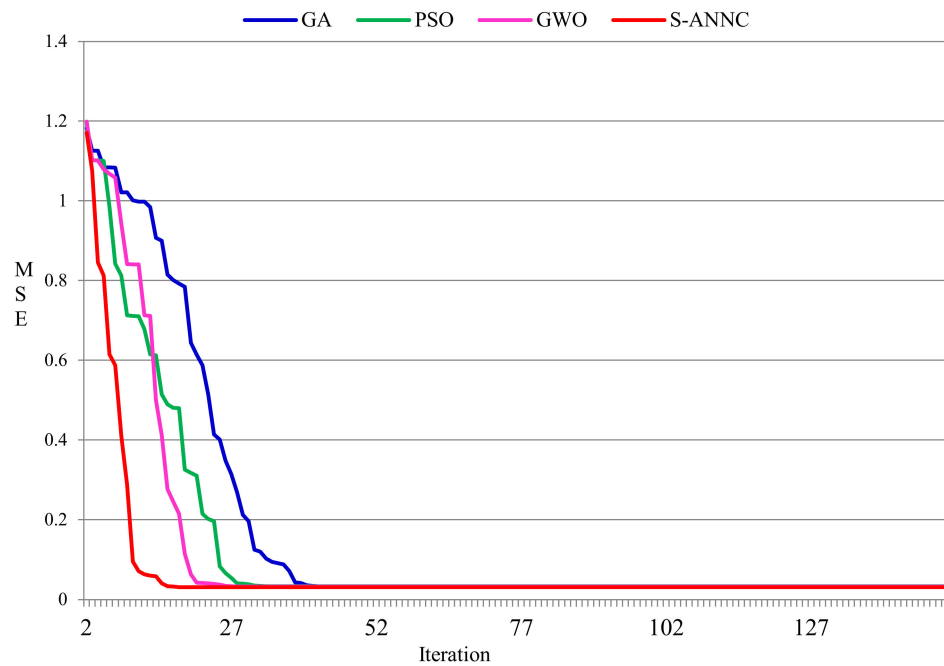


Figure 14. Comparison of convergence characteristics for case 1.

The supply voltage is balanced for case studies 1 to 3, and unbalanced for 4 and 5, respectively, with various combinations of swelling, sagging, and disturbance voltages, variable irradiation levels, and constant temperatures. In addition, the THD obtained for all of the case studies of the proposed S-ANNC is further compared with those GA, PSO, and GWO trained techniques, and with the methods that are available in the literature, as shown in Table 7. The PF is calculated from the THD using Equation (34) for all considered case studies, as shown in Figure 15.

$$PF = \cos \theta * \frac{1}{\sqrt{1 + THD^2}} \tag{34}$$

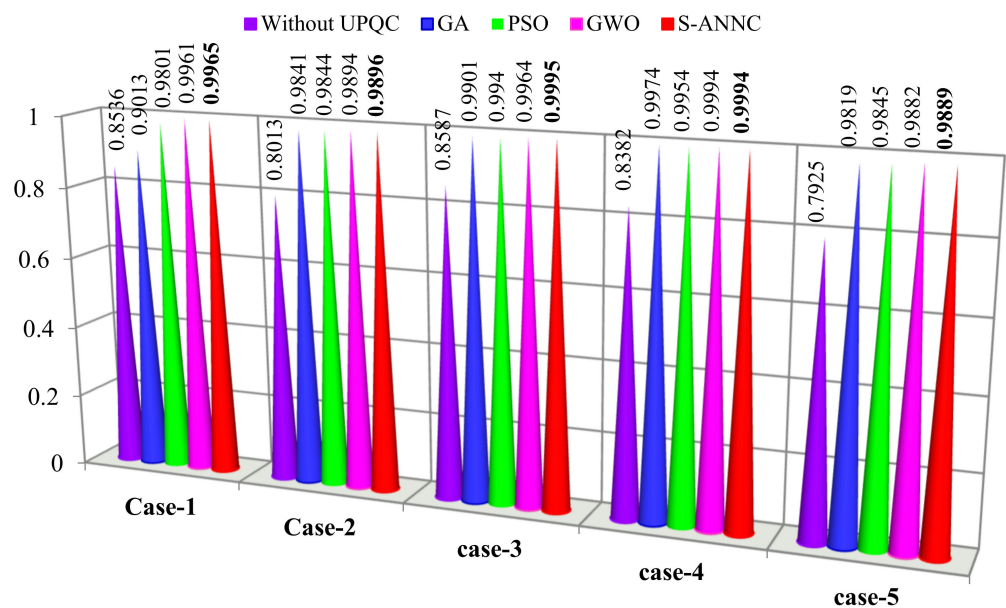


Figure 15. PF for test cases.

Table 7. THD comparison, in terms of percentage, of the proposed controller with those available in the literature.

Method	Case1	Case2	Case3	Case4	Case5
Without UPQC	27.87	16.80	19.91	9.33	21.89
GA	4.09	4.38	3.74	3.57	4.29
PSO	3.05	3.49	3.02	2.96	4.32
GWO	3.54	3.76	2.95	2.96	4.68
PSO [10]	3.75	–	–	–	–
GWO [10]	3.57	–	–	–	–
PSO-GWO [10]	3.52	–	–	–	–
PIC [25]	3.88	–	–	–	–
ACO-PIC [25]	3.72	–	–	–	–
BF-PIC [25]	3.71	–	–	–	–
PSO [23]	2.90	–	–	–	–
ZN [23]	7.57	–	–	–	–
ICM [23]	4.2	–	–	–	–
PIC [18]	3.48	–	–	–	–
PIC [20]	14.74	–	–	–	–
ANFIS [20]	6.13	–	–	–	–
PIC [22]	2.43	–	–	–	–
FLC [22]	3.65	–	–	–	–
ASO [29]	2.52	–	–	–	–
S-ANNC	2.40	3.42	2.67	2.94	3.43

Here, θ is the measured angle between the voltage and current, whereas $\frac{1}{\sqrt{1+THD^2}}$ represents the displacement factor.

The sag or swell in voltage ($V_{sag/swell}$) is calculated using Equation (35).

$$V_{sag/swell} = \frac{V_l - V_S}{V_l} = \frac{V_{se}}{V_l} \quad (35)$$

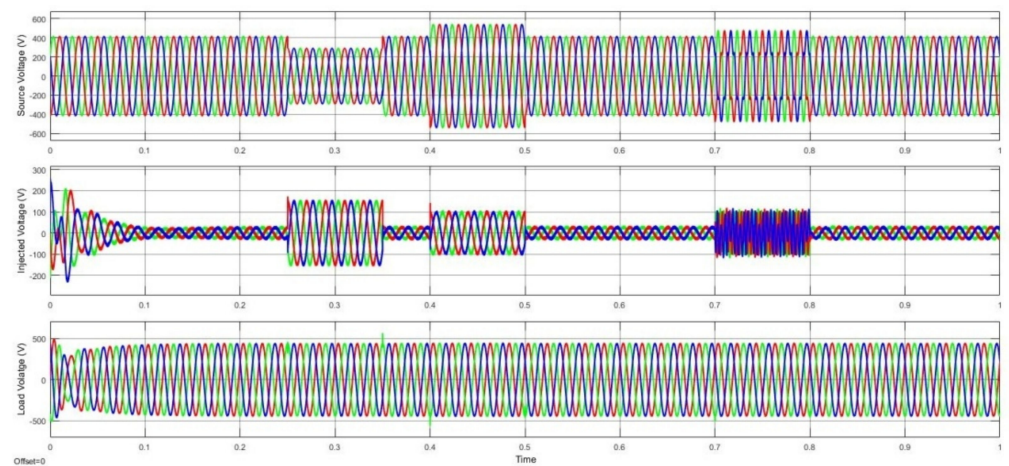
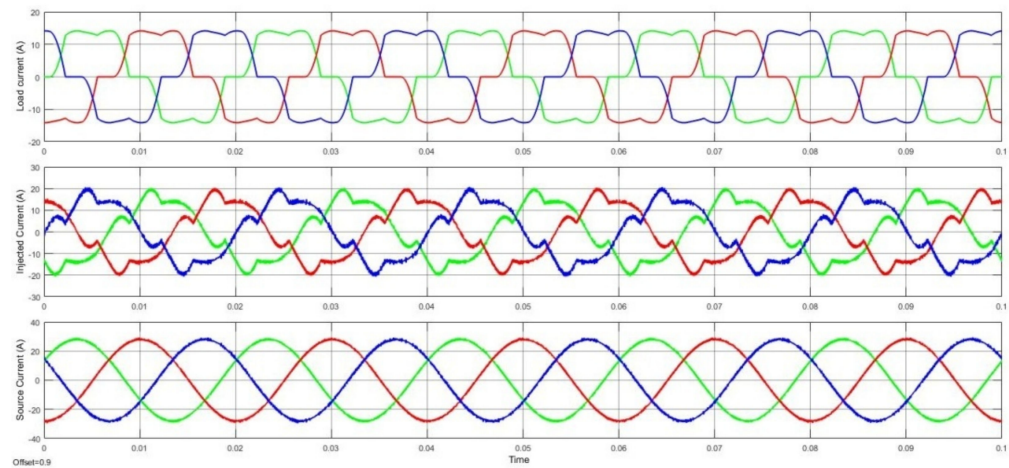
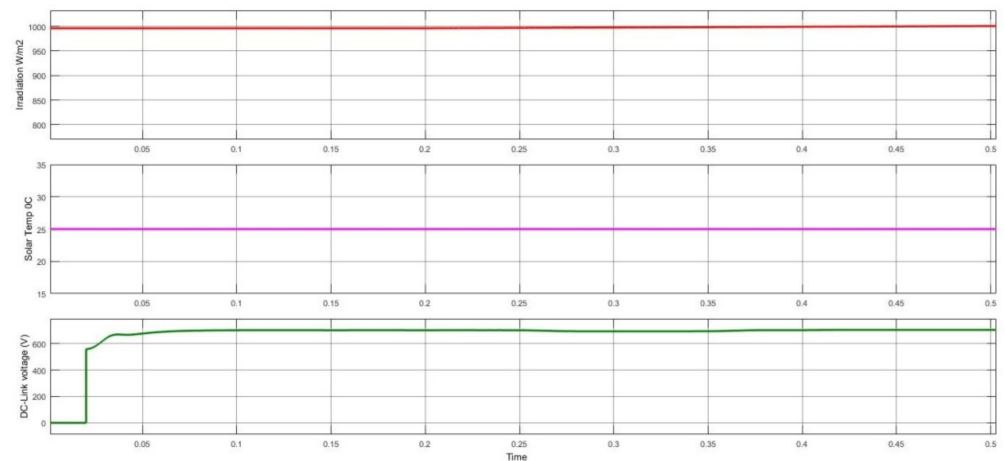
The voltage injected by the series compensator of the U-SPBS is shown in Equation (36).

$$V_{se} = V_l - V_S \quad (36)$$

The current injected by the shunt compensator is shown in Equation (37).

$$i_{sh} = i_i - i_S \quad (37)$$

In case 1, the supply voltage was balanced, and it sagged by 30% during the interval 0.25–0.35 s, and it swelled by 30% during the period 0.40–0.50 s. In addition, a disturbance was also introduced between 0.7 and 0.8 s, as illustrated in Figure 16a. The load current waveform was observed as being non-sinusoidal and balanced due to the nonlinear rectifier load, as presented in Figure 16b; however, it is clear that the U-SPBS can effectively eliminate voltage-related and current-related PQ issues by injecting a suitable compensatory voltage and current. Such an improvement in terms of the shapes of waveforms were also seen in the THD and PF values; therefore, the current THD decreased from 27.87% to 2.40%, which is a smaller decrease than those of other methods, as shown in Table 6, and the PF rose from 0.8536 to 0.9965 by injecting the required series voltages and shunt currents. In addition, the suggested controller provides a stable DC-link voltage, as shown in Figure 16c.

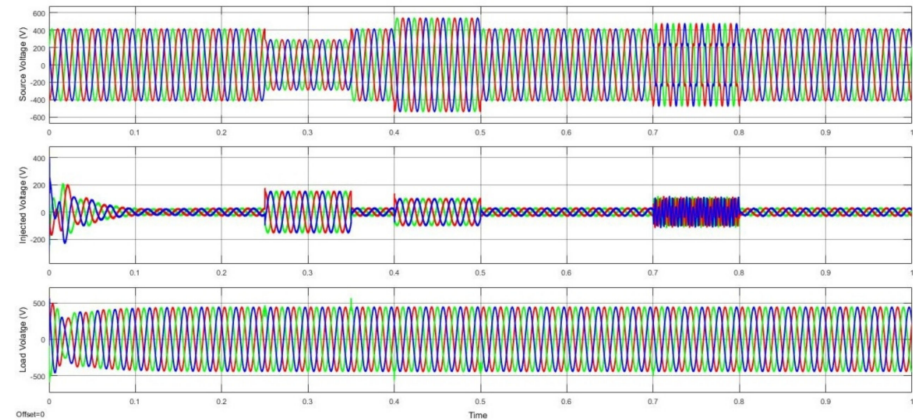
(a) V_S, V_{se}, V_l (b) i_l, i_{sh}, i_S 

(c) Solar irradiation, temperature, DC-link voltage

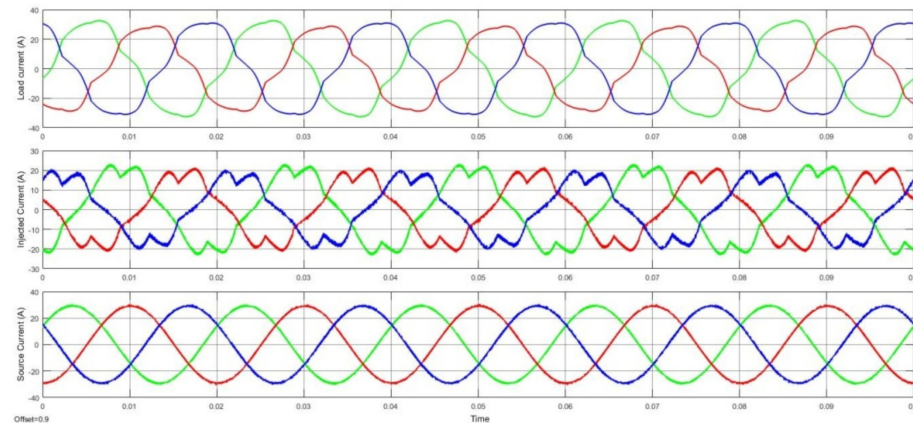
Figure 16. Waveforms of U-SPBS for case 1.

In case 2, the supply voltage was balanced with voltage-related issues, as with case 1; this is shown in Figure 17a. Here, the load current waveform was observed to be non-sinusoidal and unbalanced due to the non-linear balanced and unbalanced loads acting simultaneously, as presented in Figure 17b. It is clearly visible from the waveforms that the U-SPBS was able to manage voltage-related PQ problems effectively, and reduce THD from 16.80% to 3.42%, thereby boosting the PF value from 0.8013 to 0.9896 by injecting

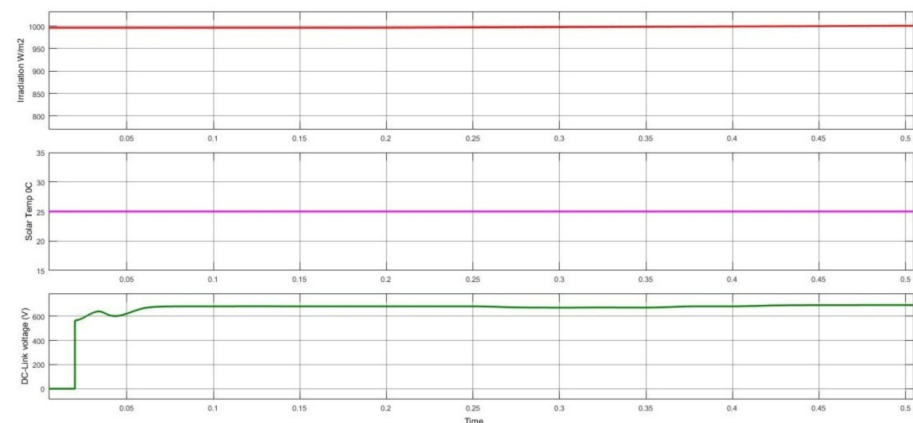
suitable compensatory voltages and currents; however, as demonstrated in Figure 17b, the suggested controller works efficiently in terms of maintaining a constant DC-link voltage, even when the load varies.



(a) V_S, V_{se}, V_l



(b) i_l, i_{shv}, i_S

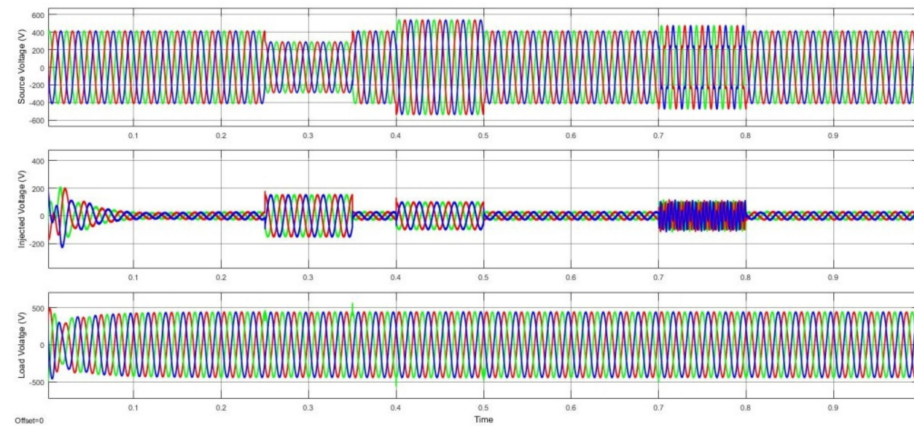


(c) Solar irradiation, temperature, DC-link voltage

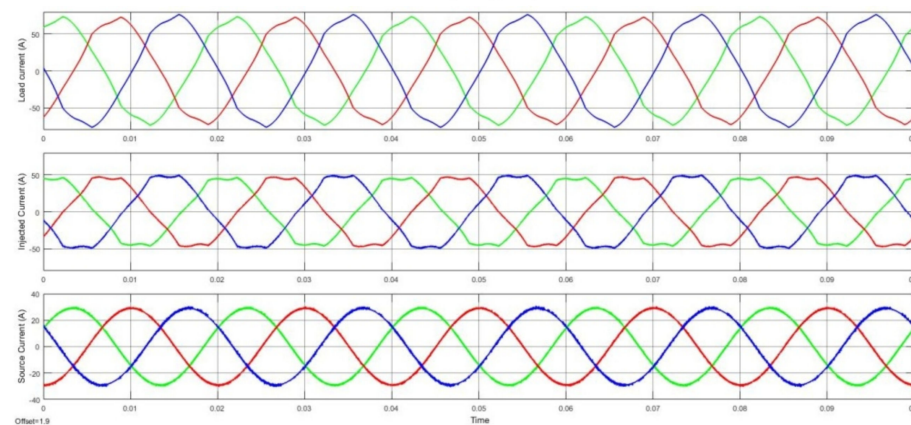
Figure 17. Waveforms of U-SPBS for case 2.

In case 3, the supply voltage was balanced using a combination of a 3ϕ balanced rectifier load and an unbalanced and induction furnace load; these loads were simultaneously injected, and are shown in Figure 18a. The load current was observed to be highly non-sinusoidal and balanced, as shown in Figure 18b; however, the S-ANNC was able to successfully suppress the THD from 19.91% to 2.67%, improve the PF from 0.8587 to 0.9995, and balance the load voltage by injecting suitable appropriate currents and voltages into

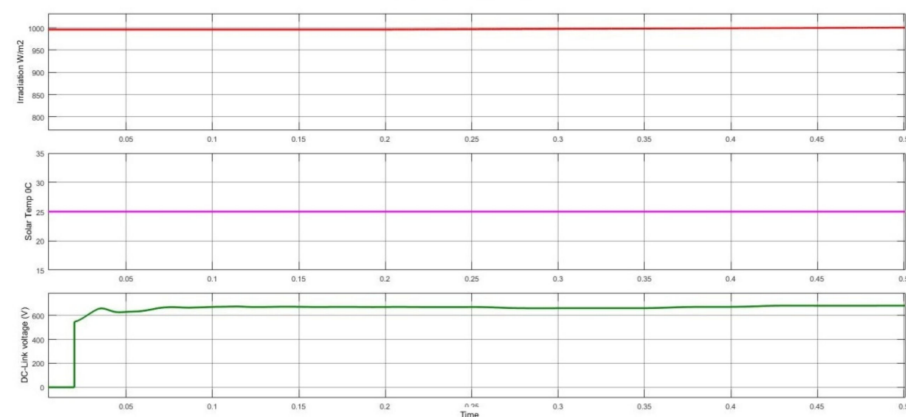
the network. In addition, it also stabilized the DC-link voltage after the introduction of the large non-linear load, as shown in Figure 18c.



(a) V_S, V_{se}, V_l



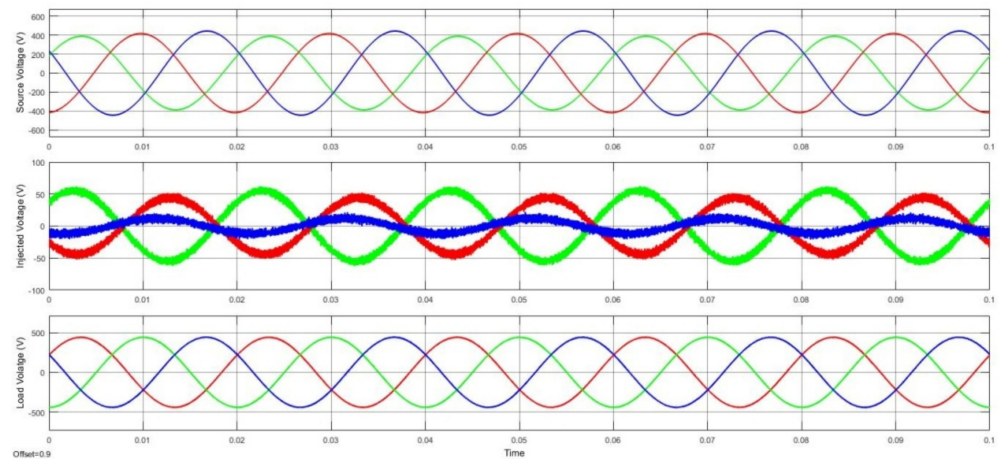
(b) i_l, i_{shr}, i_S



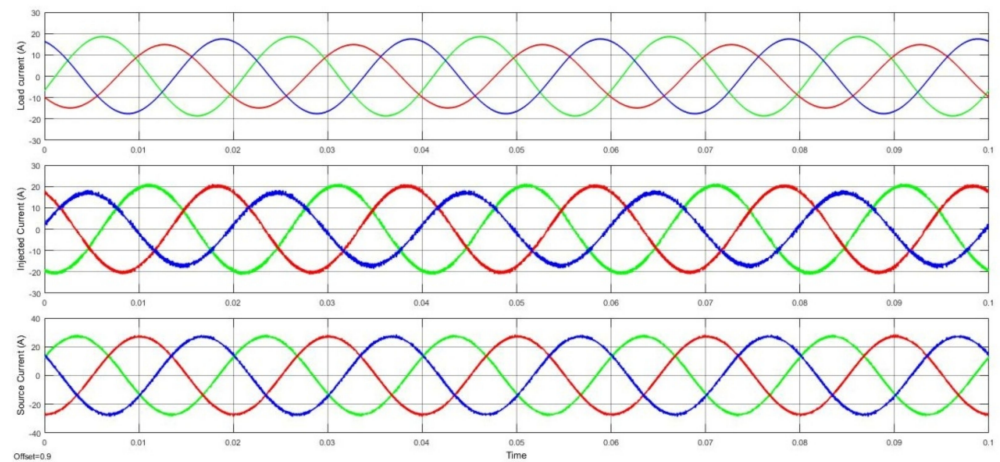
(c) Solar irradiation, temperature, DC-link voltage

Figure 18. Waveforms of U-SPBS for case 3.

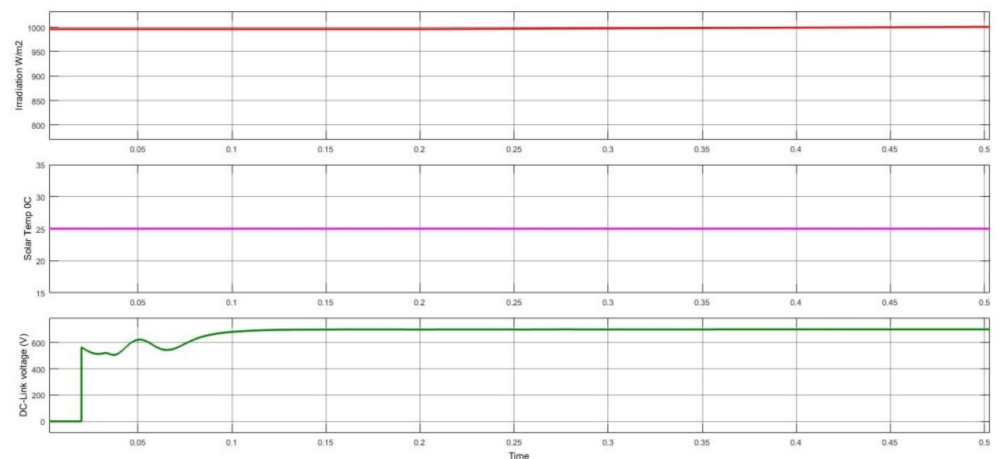
In case 4, the supply voltage and load were both unbalanced, as shown in Figure 19a. The load current waveforms were observed to be sinusoidal, but unbalanced, as shown in Figure 19b. The S-ANNC suppressed the harmonics in the current waveform and decreased the THD from 9.33% to 2.94%. The PF was boosted from 0.83872 to 0.9994. Figure 19c shows its performance in terms of its ability to regulate the DC-link voltage when the load varies.



(a) V_S, V_{se}, V_l



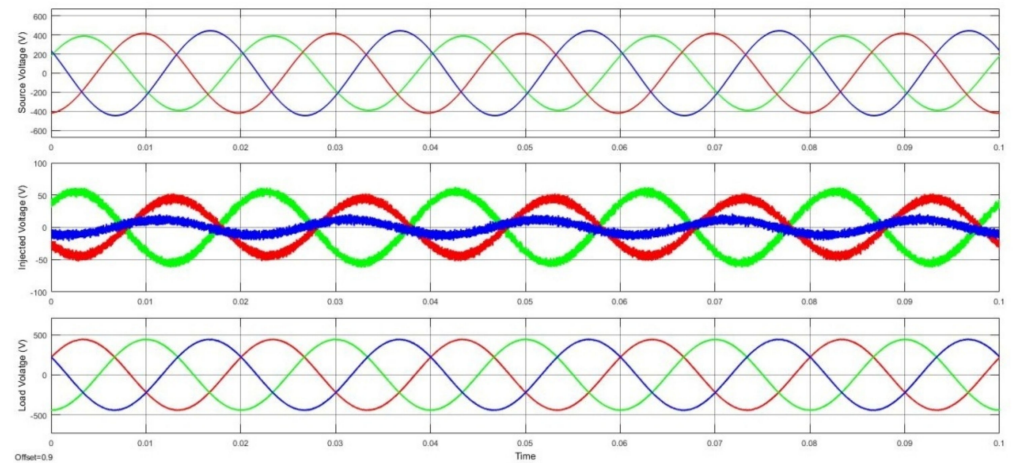
(b) i_l, i_{sh}, i_S



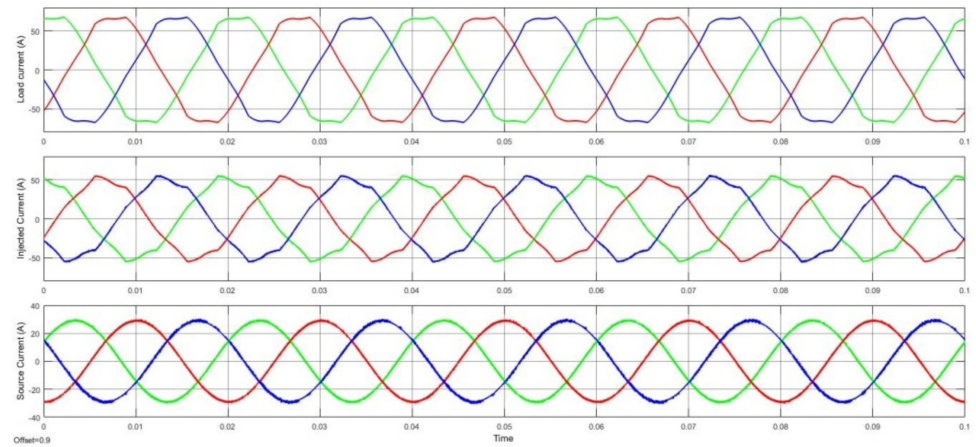
(c) Solar irradiation, temperature, DC-link voltage

Figure 19. Waveforms of U-SPBS for case 4.

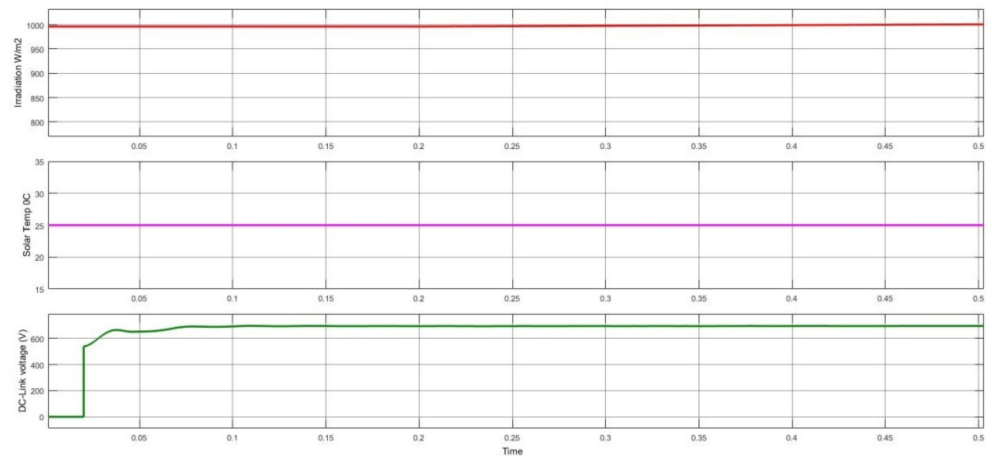
In case 5, the unbalanced supply voltage was considered using a combination of 3ϕ rectifier and induction furnace loads, as shown in Figure 20a. The load current was balanced with a non-sinusoidal structure, as shown in Figure 20b. The suggested S-ANNC effectively diminished the THD level, from 21.89% to 3.43%, and boosted the PF from 0.7925 to 0.9889; however, the stability of the DC-link voltage was maintained, as shown in Figure 21, during the dynamic variation in solar irradiation, under constant temperature and load conditions.



(a) V_S, V_{se}, V_l



(b) i_l, i_{sh}, i_S



(c) Solar irradiation, temperature, DC-link voltage

Figure 20. Waveforms of U-SPBS for case 5.

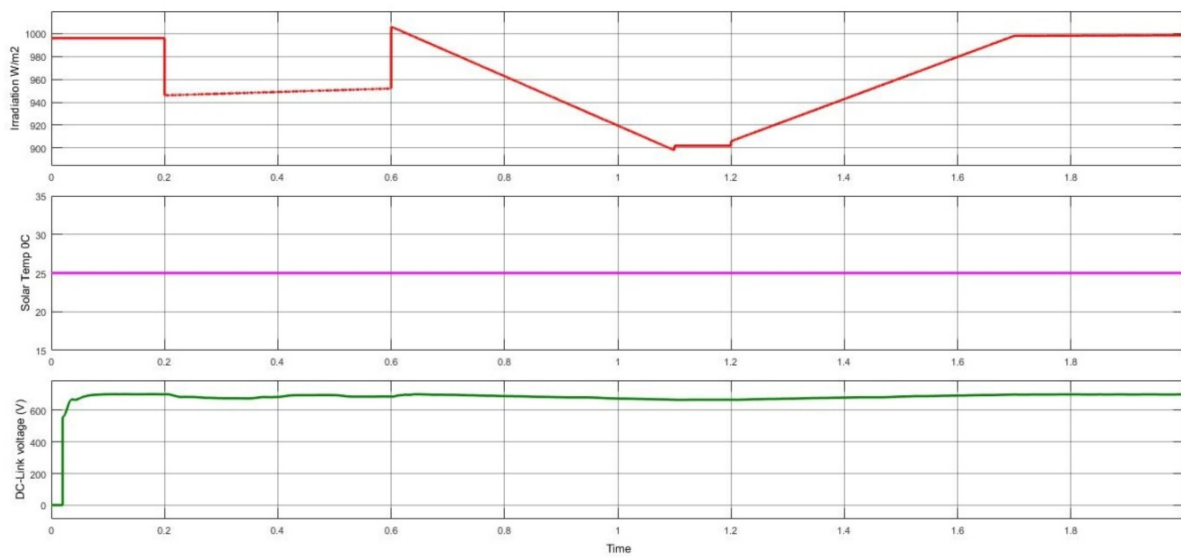


Figure 21. Waveforms for U-SPBS under constant load conditions during solar irradiation variation, a constant temperature of 25 °C, and DC-link voltage.

In Figure 14, it can clearly be seen that the proposed controller converges to allow for a lower MSE, in a smaller number of iterations, when compared to other techniques. Table 8 provides a comparison of MSEs, examining the proposed method with those used in other techniques. Figure 21 also proves that the proposed controller can provide a constant DC-link voltage when irradiation levels vary under constant temperature conditions. The proof of accuracy for the proposed S-ANNC with a regression plot is shown in Figure 22. The THD spectrum for all test cases is shown in Figure 23.

Table 8. Comparison of MSEs.

Case	Method	MSE
1	GA	0.03386
	PSO	0.03322
	GWO	0.03290
	S-ANNC	0.03107
2	GA	0.01622
	PSO	0.01656
	GWO	0.01496
	S-ANNC	0.01457
3	GA	0.01500
	PSO	0.01168
	GWO	0.01608
	S-ANNC	0.01107
4	GA	0.00402
	PSO	0.00413
	GWO	0.00146
	S-ANNC	0.00142
5	GA	0.04626
	PSO	0.05130
	GWO	0.04390
	S-ANNC	0.04387

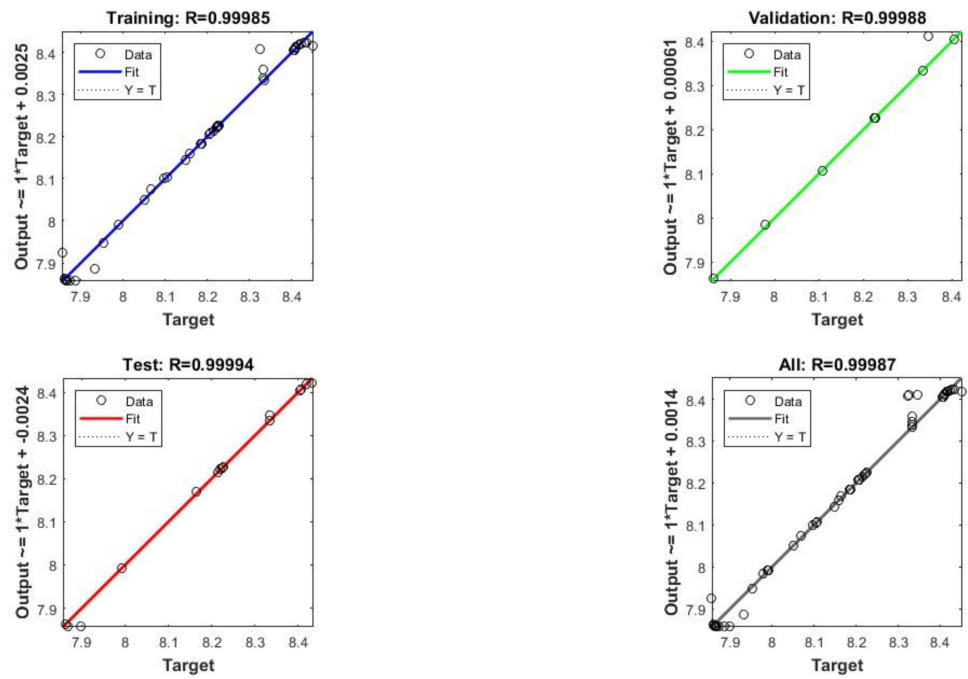


Figure 22. Proof of accuracy for the proposed S-ANNC with a regression plot.

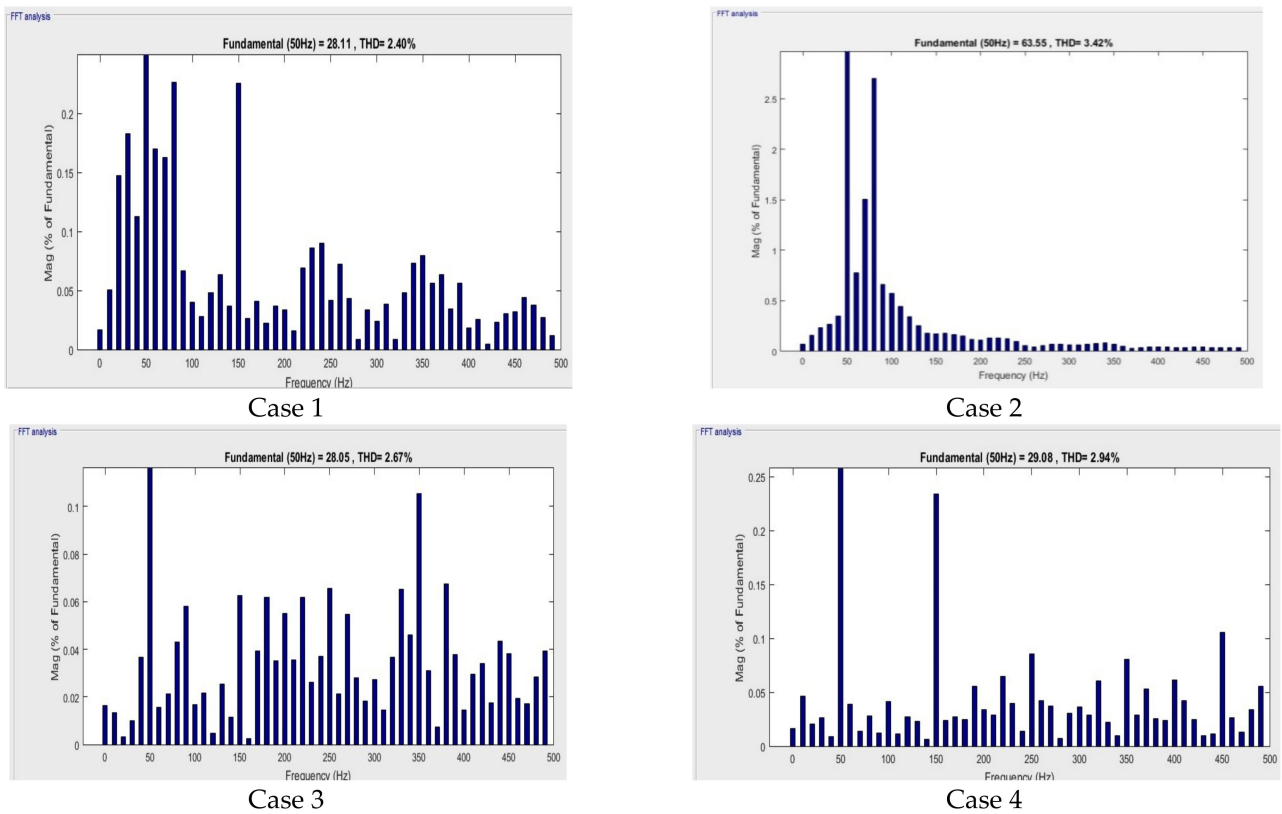
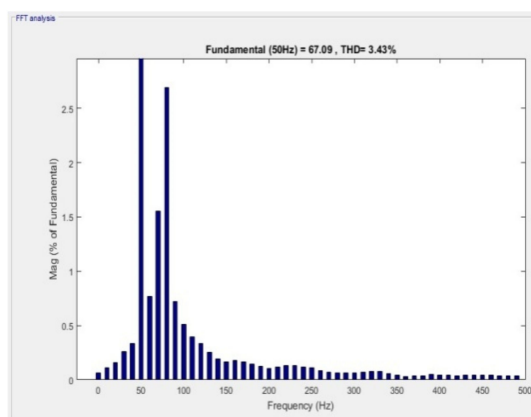


Figure 23. Cont.



Case 5

Figure 23. THD spectrum for the case studies.

5. Conclusions

The hybrid controller, which used a combination of FLC and optimally trained ANN properties, was proposed in this paper for use in a U-SPBS. The design of the controllers for the SPV and BS were also specified, in addition to the development of S-ANNC for SUAPF, and FLC for SEAPF. This was done with the aim of:

1. Attaining rapid action when stabilizing the DC-link capacitance voltage, with the intention of achieving a minimum settling time.
2. Eliminating swelling, sagging, and disturbances in the supply voltage.
3. Suppressing the harmonics in the source current and boosting the PF by aiming to minimize the MSE.

From the investigation of the five test cases, it is clear that the proposed method was able to reduce the THDs to 2.40%, 3.42%, 2.67%, 2.94%, and 3.43% for the five test cases, and the PF was also reduced to a similar level. Moreover, in accordance with the comparative analysis, it has been proven that the performance of the proposed controller was much better than the GA, PSO, and GWO controllers. It also effectively maintains a stable voltage across the DC-link when load and solar irradiation varies. The proposed system can be studied further in a future study, using a multi-level UPQC with a micro-grid in the distribution network.

Author Contributions: Data curation: P.K.B. and K.S.; Writing original draft: K.S.; Supervision: L.M.-P. and P.K.B.; Project administration: P.K.B., K.S. and L.M.-P.; Conceptualization: C.N.S. and N.U.K.; Methodology: C.N.S. and K.S.; Validation: N.U.K. and C.N.S.; Visualization: C.N.S. and N.U.K.; Resources: L.M.-P. and P.K.B.; Review & Editing: L.M.-P., P.K.B. and K.S.; Funding acquisition: L.M.-P. All authors have read and agreed to the published version of the manuscript.

Funding: This research received no external funding.

Institutional Review Board Statement: Not applicable.

Informed Consent Statement: Not applicable.

Data Availability Statement: Not applicable.

Conflicts of Interest: The authors declare no conflict of interest.

Nomenclature

UPQC	Unified power quality conditioner
SUAPF	Shunt active power filter
SEAPF	Series active power filter
ANNC	Artificial neural network controller
SOLO	Soccer League algorithm

S-ANNC	Soccer League algorithm trained ANN Controller
GA	Genetic algorithm
PSO	Particle swarm optimization
GWO	Grey wolf optimization
PQ	Power Quality
UPQC	Unified Power Quality Conditioner
SPV	Solar Photovoltaic
BS	Battery Storage
BP	Back Propagation
LM	Levenberg–Marquardt
MLP	Multi-layer perceptron
IL	Input layer
HL	Hidden layer
OL	Output layer
FLC	Fuzzy Logic Controller
PIC	Proportional Integral Controller
SMC	Sliding-mode Controller
SYP	Synchronization of Phases
STF	Self-Tuning Filter
UVGM	Unit Vector Generation Method
PLL	Phase-Locked-Loop
LPF	Low-Pass Filter
HPF	High-Pass Filter
FC	Fundamental component
HC	Harmonic component
PF	Power Factor
IOT	Internet of Things
DSTATCOM	Distributed static compensator
DPD	DC-link power demand
MF	Membership Functions
SRFT	Synchronous Reference Frame Theory
BC	Boost Converter
BBC	Buck–Boost Converter
SPG	Solar Power Generated
MSE	Mean square error
$V_{S_a}, V_{S_b}, V_{S_c}$	Source voltage for abc phases
$i_{S_a}, i_{S_b}, i_{S_c}$	Source current for abc phases
$V_{S_\alpha}, V_{S_\beta}, V_{S_0}$	Source voltage in α_β_0 domain
$V'_{S_\alpha}, V'_{S_\beta}, V'_{S_0}$	FC of source voltage in α_β_0 domain
R_S	Source-Resistance
L_S	Source-Inductance
$V_{L_a}, V_{L_b}, V_{L_c}$	Load voltage for a, b, c phases
$V_{se_a}, V_{se_b}, V_{se_c}$	Series injected voltage for a, b, c phases
$V^{ref}_a, V^{ref}_b, V^{ref}_c$	Reference voltages for a, b, c phases
$V^{ref}_{se_d}, V^{ref}_{se_q}$	Series injected reference voltage in d_q domain
$V^{ref}_{se_\alpha}, V^{ref}_{se_\beta}$	Series injected reference voltage in α_β domain
$V^{ref}_\alpha, V^{ref}_\beta$	Reference voltage in α_β domain
V^{ref}_d, V^{ref}_q	Reference voltage in d_q domain
$i_{L_a}, i_{L_b}, i_{L_c}$	Load current for phase a, b, c
$i_{L_\alpha}, i_{L_\beta}, i_{L_0}$	Load currents in α_β_0 domain
$i'_{L_\alpha}, i'_{L_\beta}, i'_{L_0}$	FC of load currents in α_β_0 domain
$i''_{L_\alpha}, i''_{L_\beta}, i''_{L_0}$	HC of load current in α_β_0 domain
i''_{L_d}, i''_{L_q}	HC of load current in d_q domains
$i^{ref}_{L_a}, i^{ref}_{L_b}, i^{ref}_{L_c}$	Reference load current for phases abc
$i^{ref}_{L_\alpha}, i^{ref}_{L_\beta}, i^{ref}_{L_0}$	Reference load current α_β_0 domain
$i^{ref}_{L_d}, i^{ref}_{L_q}$	Reference load current in d_q domain
$i_{sh_a}, i_{sh_b}, i_{sh_c}$	SUAPF injected current for a, b, c phases

$i_{sh_a}^{ref}, i_{sh_b}^{ref}, i_{sh_c}^{ref}$	Reference SUAPF injected current for abc phases
$i_{sh_a}, i_{sh_b}, i_{sh_c}$	SUAPF injected current for abc phases
C_{sh}	SUAPF Capacitance
R_{sh}	SUAPF Resistance
L_{sh}	SUAPF Inductance
C_{dc}	Capacitance of the capacitor across DC-Link
V_{dc}	Actual voltage of DC-link capacitor
$V_{dc,error}$	DC-link error voltage
V_{dc}^{ref}	Reference voltage of DC-Link capacitor
Δi_{dc}	DC-link output error
i_{dc}^{ref}	DC-link reference current
P_{PV}	Solar PV output power
V_{PV}	Solar output voltage
I_{PV}	Solar output current
P_{DC}	Power at DC-link
P_{BS}	Battery Power
V_{BS}	Battery voltage
i_{BS}	Battery current
i_{BS}^{ref}	Battery reference current
$i_{BS,error}$	Battery error current
$i_{BS,error}^*$	Battery reference error current
Q	Battery capacity
E	Error
CE	Change in error
$SOCB$	State of charge of battery

References

- Gali, V.; Gupta, R.N.; Gupta, A. Mitigation of power quality problems using shunt active power filters: A comprehensive review. In Proceedings of the 12th IEEE Conference on Industrial Electronics and Applications (ICIEA), Siem Reap, Cambodia, 18–20 June 2017.
- Kesler, M.; Ozdemir, E. Synchronous-Reference-Frame-Based Control Method for UPQC Under Unbalanced and Distorted Load Conditions. *IEEE Trans. Ind. Electron.* **2010**, *58*, 3967–3975. [[CrossRef](#)]
- Suresh, M.; Panda, A.K. PI and Fuzzy Logic Controller based 3-phase 4-wire Shunt active filter for mitigation of Current harmonics with Id-Iq Control Strategy. *J. Power Electron.* **2011**, *11*, 914–921. [[CrossRef](#)]
- Soumya, R.; Das Prakash, K.; Ray Asit, M.; Gayadhar, P. Power Quality Enhancement in PV and Battery Storage Based Microgrid Using Hybrid Active Filter. In Proceedings of the 2020 3rd International Conference on Energy, Power and Environment: Towards Clean Energy Technologies, Meghalaya, India, 5–7 March 2021.
- Suresh, M.; Panda, A.K. RTDS hardware implementation and simulation of SHAF for mitigation of harmonics using p-q control strategy with PI and Fuzzy logic controllers. *Front. Electr. Electron. Eng.* **2021**, *7*, 427–437. [[CrossRef](#)]
- Lin, H.C. Intelligent Neural Network-Based Fast Power System Harmonic Detection. *IEEE Trans. Ind. Electron.* **2007**, *54*, 43–52. [[CrossRef](#)]
- Dash, P.K.; Panda, S.K.; Lee, T.H.; Xu, J.X.; Tray, A.R. Fuzzy and Neural Controllers for Dynamic Systems: An Overview. In Proceedings of the Second International Conference on Power Electronics and Drive Systems, Singapore, 26–29 May 1997.
- Devassy, S.; Singh, B. Design and Performance Analysis of Three-Phase Solar PV Integrated UPQC. *IEEE Trans. Ind. Appl.* **2017**, *54*, 73–81. [[CrossRef](#)]
- Krishna, V.K.; Dash, S.K.; Geshma, K.R. Development and Analysis of Power Quality by using Fuel cell based Shunt Active Power Filter. In Proceedings of the 2020 2nd International Conference on Innovative Mechanisms for Industry Applications (ICIMIA), Bangalore, India, 5–7 March 2020.
- Mishra, A.K.; Das, S.S.; Ray, P.K.; Ranjan, K.M.; Asit, M.; Dillip, K.M. PSO-GWO Optimized Fractional Order PID Based Hybrid Shunt Active Power Filter for Power Quality Improvements. *IEEE Access* **2022**, *8*, 74497–74512. [[CrossRef](#)]
- Chandrasekaran, K.; Selvaraj, J.; Amaladoss, C.R.; Veerapan, L. Hybrid renewable energy based smart grid system for reactive power management and voltage profile enhancement using artificial neural network. *Energy Sources Part A Recover. Util. Environ. Eff.* **2021**, *43*, 2419–2442. [[CrossRef](#)]
- Srilakshmi, K.; Srinivas, N.; Balachandran, P.K.; Reddy, G.P.; Gaddameddi, S.; Valluri, N.; Selvarajan, S. Design of Soccer League Optimization Based Hybrid Controller for Solar-Battery Integrated UPQC. *IEEE Access* **2022**, *10*, 107116–107136. [[CrossRef](#)]
- Sarker, K.; Chatterjee, D.; Goswami, S.K. A modified PV-wind-PEMFCS-based hybrid UPQC system with combined DVR/STATCOM operation by harmonic compensation. *Int. J. Model. Simul.* **2020**, *41*, 243–255. [[CrossRef](#)]

14. Koganti, S.; Koganti, K.J.; Salkuti, S.R. Design of Multi-Objective-Based Artificial Intelligence Controller for Wind/Battery-Connected Shunt Active Power Filter. *Algorithms* **2022**, *15*, 256. [[CrossRef](#)]
15. Srilakshmi, K.; Babu, P.R.; Venkatesan, Y.; Palanivelu, A. Soccer league optimization for load flow analysis of power systems. *Int. J. Numer. Model. Electron. Netw. Devices Fields* **2021**, *35*, e2965. [[CrossRef](#)]
16. Abdusalam, M.; Poure, P.; Karimi, S.; Saadate, S. New digital reference current generation for shunt active power filter under distorted voltage conditions. *Electr. Power Syst. Res.* **2009**, *79*, 759–765. [[CrossRef](#)]
17. Almelian, M.; Mohd, I.; Omran, M.; Sheikh, U. Performance of unified power quality conditioner (UPQC) based on fuzzy controller for attenuating of voltage and current harmonics. *IOP Conf. Ser. Mater. Sci. Eng.* **2018**, *3*, 12–84.
18. Samal, S.; Hota, P.K. Design and analysis of solar PV-fuel cell and wind energy based microgrid system for power quality improvement. *Cogent Eng.* **2017**, *4*, 1402453. [[CrossRef](#)]
19. Sayed, J.A.; Sabha, R.A.; Ranjan, K.J. Biogeography based optimization strategy for UPQC PI tuning on full order adaptive observer based control. *IET Gener. Transm. Distrib.* **2021**, *15*, 279–293.
20. Renduchintala, U.K.; Pang, C.; Tatikonda, K.M.; Yang, L. ANFIS-fuzzy logic based UPQC in interconnected microgrid distribution systems: Modeling, simulation and implementation. *J. Eng.* **2021**, *2021*, 6–18. [[CrossRef](#)]
21. Rajesh, P.; Shajin, F.H.; Umasankar, L. A Novel Control Scheme for PV/WT/FC/Battery to Power Quality Enhancement in Micro Grid System: A Hybrid Technique. *Energy Sources Part A Recover. Util. Environ. Eff.* **2021**, 1–18. [[CrossRef](#)]
22. Pazhanimuthu, C.; Ramesh, S. Grid integration of renewable energy sources (RES) for power quality improvement using adaptive fuzzy logic controller based series hybrid active power filter (SHAPF). *J. Intell. Fuzzy Syst.* **2018**, *35*, 749–766. [[CrossRef](#)]
23. Mahaboob, S.; Ajithan, S.K.; Jayaraman, S. Optimal design of shunt active power filter for power quality enhancement using predator-prey based firefly optimization. *Swarm Evol. Comput.* **2019**, *44*, 522–533. [[CrossRef](#)]
24. Faris, H.; Aljarah, I.; Al-Madi, N.; Mirjalili, S. Optimizing the Learning Process of Feedforward Neural Networks Using Lightning Search Algorithm. *Int. J. Artif. Intell. Tools* **2016**, *25*, 1650033. [[CrossRef](#)]
25. Sakthivel, A.; Vijayakumar, P.; Senthilkumar, A.; Lakshminarasimman, L.; Paramasivam, S. Experimental investigations on Ant Colony Optimized PI control algorithm for Shunt Active Power Filter to improve Power Quality. *Control Eng. Pract.* **2015**, *42*, 153–169. [[CrossRef](#)]
26. Nagireddy, V.V.; Kota, V.R.; Kumar, D.A. Hybrid fuzzy back-propagation control scheme for multilevel unified power quality conditioner. *Ain Shams Eng. J.* **2018**, *9*, 2709–2724. [[CrossRef](#)]
27. Yamany, W.; Tharwat, A.; Hassanin, M.F.; Gaber, T.; Hassanien, A.E.; Kim, T.-H. A new multi-layer perceptrons trainer based on ant lion optimization algorithm. In Proceedings of the 2015 Fourth International Conference on Information Science and Industrial Applications, Busan, Korea, 20–22 September 2015. [[CrossRef](#)]
28. Hassanin, M.F.; Shoeb, A.M.; Hassanien, A.E. Grey Wolf Optimizer-based Back-propagation Neural Network Algorithm. In Proceedings of the 12th International Computer Engineering Conference (ICENCO), Cairo, Egypt, 29–30 December 2022. [[CrossRef](#)]
29. Goud, B.S.; Rao, B.L. Power Quality Enhancement in Grid-Connected PV/Wind/Battery Using UPQC: Atom Search Optimization. *J. Electr. Eng. Technol.* **2021**, *16*, 821–835. [[CrossRef](#)]